

Ozone and carbon monoxide over India during the summer monsoon: regional emissions and transport

N. Ojha, A. Pozzer, A. Rauthe-Schöch, A. K. Baker, J. Yoon, C. A. M. Brenninkmeijer, and J. Lelieveld

Atmospheric Chemistry Department, Max Planck Institute for Chemistry, Mainz, Germany

Correspondence to: N. Ojha (narendra.ojha@mpic.de)

Abstract

We compare in situ measurements of ozone (O_3) and carbon monoxide (CO) profiles from the CARIBIC program with the results from the regional chemistry transport model (WRF-Chem) to investigate the role of local/regional emissions and long-range transport over southern India during the summer monsoon of 2008. WRF-Chem successfully reproduces the general features of O_3 and CO distributions over the South Asian region. However, absolute CO concentrations in the lower troposphere are typically underestimated. Here we investigate the influence of local relative to remote emissions through sensitivity simulations.

The influence of 50 % increased CO emissions over South Asia leads to a significant enhancement (upto 20 % in July) in upper tropospheric CO in the northern and central Indian regions. Over Chennai in southern India, this causes a 33 % increase in surface CO during June. However, the influence of enhanced local /regional emissions is found to be smaller (5 %) in the free troposphere over Chennai, except during September. Local to regional emissions are therefore suggested to play a minor role in the underestimation of CO by WRF-Chem during June–August. In the lower troposphere, a high pollution (O_3 : $146.4 \pm 12.8 \text{ nmol mol}^{-1}$, CO: $136.4 \pm 12.2 \text{ nmol mol}^{-1}$) event (15 July 2008), not reproduced by the model, is shown to be due to transport of photochemically processed air masses from the boundary layer in southern India. A sensitivity simulation combined with backward trajectories indicates that long-range transport of CO to southern India is significantly underestimated, particularly in air masses from the west, i.e. from Central Africa. This study highlights the need for more aircraft-based measurements over India and adjacent regions and the improvement of global emission inventories.

1 Introduction

Tropospheric ozone and its precursors play vital roles in atmospheric chemistry, air quality degradation and climate change (e.g. WHO, 2003; Stevenson et al., 2013; Monks et al., 2014). It is therefore important to understand the spatial and temporal distributions of these

species and the contributions of different sources to their atmospheric budgets. Additionally, relative contributions of regional anthropogenic emissions and long-range transport need to be addressed for adequate policy making. In order to understand the quantitative contributions of different sources and processes (chemistry, transport) to the budgets of trace gases, systematic measurements of the vertical distribution of trace species are required in conjunction with chemistry-transport modeling.

Unfortunately, in situ measurements of vertical distribution of ozone and related trace gases are very sparse over the South Asian region, where rapidly increasing anthropogenic emissions lead to severe air pollution in recent years (e.g. Akimoto, 2003; Beig and Brasseur, 2006; Ohara et al., 2007; Lelieveld et al., 2013; Pozzer et al., 2015). It is suggested that air quality will further deteriorate to become severe over India in a Business-as-Usual (BAU) scenario (Pozzer et al., 2012). A recent study shows that ozone pollution alone could lead to a loss of crop yield which could feed 94 million people below the poverty threshold in India (Ghude et al., 2014). Observations such as the Indian Ocean Experiment (INDOEX) (Lelieveld et al., 2001) and the Integrated Campaign for Aerosols, Gases and Radiation Budget (ICARB) (Srivastava et al., 2011) have revealed significant South Asian outflow over the surrounding marine regions (Lawrence and Lelieveld, 2010, and references therein). Additionally, the emissions and photochemically processed air masses can be up-lifted due to strong tropical convection and can be transported to distant regions (Lelieveld et al., 2002; Lawrence et al., 2003; Park et al., 2007) influencing global air quality and climate.

Numerous efforts have been initiated to conduct in situ ground-based measurements of ozone and precursors (e.g. Lal et al., 2000; Reddy et al., 2008; David and Nair, 2011; Sarangi et al., 2014) as well as ship-based measurements (e.g. Sahu and Lal, 2006; Mallik et al., 2013; Lawrence and Lelieveld, 2010, and references therein). However, most of the studies over this region have been confined to the surface. The observational studies were followed by utilizing global chemistry-transport models, such as MATCH-MPIC (Lal and Lawrence, 2001; Ojha et al., 2012), MOZART (Beig and Brasseur, 2006; Sheel et al., 2010), and recently with a regional chemistry-transport model (WRF-Chem)

(Kumar et al., 2012b; Michael et al., 2014). WRF-Chem simulations were generally found to reproduce the variations observed in ground-based and ozonesonde measurements over India (Kumar et al., 2012b). Model evaluation over an urban site in the Indo-Gangetic plain (Michael et al., 2014) showed an increase in model biases in simulating O_3 and CO towards the onset of monsoon as compared to spring. Model results were also evaluated against satellite retrievals of NO_2 and CO (Kumar et al., 2012b). These studies suggested that WRF-Chem at higher resolution could better capture the variations in trace gases and aerosols than global models over the Indian region because of better dealing with the complex topography and large spatio-temporal heterogeneity in the emissions. However, evaluation of WRF-Chem simulations over the Indian region is still very limited, particularly against in situ measurements of vertical profiles (Kumar et al., 2012b).

The studies over the Indian region utilizing the WRF-Chem model have revealed significant differences between the model simulations and measurements, which have been attributed mainly to uncertainties in anthropogenic emissions (Kumar et al., 2012b; Michael et al., 2014). Transport of CO has been investigated for the winter season by evaluating the model against satellite datasets (Kumar et al., 2013) in the absence of in situ observations of vertical profiles. Lack of in situ measurements in the free troposphere and above has inhibited the quantitative understanding of the transport involved, which could play a significant role in the free troposphere (e.g. Lal et al., 2013, 2014; Ojha et al., 2014). CARIBIC (Civil Aircraft for the Regular Investigation of the Atmosphere Based on an Instrument Container) observations (<http://www.caribic-atmospheric.com/>, Brenninkmeijer et al., 2007; Rauthe-Schöch et al., 2015) can partly fill this gap by providing in situ measurements of ozone and CO profiles over the Indian region.

The Asian summer monsoon is a dominant atmospheric phenomenon over the Indian region and is shown to redistribute trace gases and aerosols (Park et al., 2009; Randel et al., 2010; Baker et al., 2011; Cristofanelli et al., 2014; Fadnavis et al., 2013, 2015). The monsoonal convection uplifts and mixes regional pollution into the upper troposphere, while the anticyclonic winds can bring polluted air masses from other regions and also export the monsoon air with its pollution to regions far away from India. However, the influences

of local and regional emissions compared to long-range transport are not well understood, primarily due to lack of in situ measurements of vertical profiles for the evaluation of model simulations. A few studies have utilized satellite datasets, however the view of satellite instruments during the monsoon period is often obscured by clouds. While global models have the advantage of including large-scale dynamics /long-range transport, the regional models offer better opportunities to investigate the effects of high-resolution regional emissions and regional photochemistry. The inflow of pollution to the regional models is generally provided in form of time-varying chemical boundary conditions from global model simulations (e.g. Pfister et al., 2013; Andersson et al., 2015). Therefore, long-range pollution transport is accounted for but at reduced time resolution compared to global models. This study utilizes CARIBIC measurements of ozone and CO profiles conducted during the summer monsoon period (June to September) in the year 2008 in conjunction with the regional chemistry transport model (WRF-Chem) to assess the contributions of emissions and long-range transport over the southern Indian region. WRF-chem simulations are evaluated against the in situ CARIBIC profiles, an ozonesonde climatology, satellite (MOPITT) retrievals and ground-based measurements to identify the strengths and limitations of the WRF-Chem simulations. Additionally, we conduct a set of sensitivity simulations to identify the role of anthropogenic emissions and long-range transport/boundary conditions.

The paper is structured as follows: the configuration of the WRF-Chem model used in the present study is described in Sect. 2. The CARIBIC measurements, satellite data and ground-based measurements used to evaluate the model simulations are discussed in Sect. 3. The results with a focus on model evaluation are presented in Sect. 4.1, followed by an investigation of the influences of regional emissions (Sect. 4.2) and transport (Sect. 4.3). The summary and conclusions are presented in Sect. 5.

2 Model description and setup

2.1 WRF-Chem

We use version 3.5.1 of the Weather Research and Forecasting with Chemistry (WRF-Chem), an online regional chemistry transport model (Grell et al., 2005). The simulation domain has been defined on the Mercator projection (Fig. 1). The model domain is centered at 80° E, 22° N, and covers nearly the entire South Asian region with a spatial resolution of 30 km × 30 km. In the west-east and south-north directions, the domain has 132 and 120 grid points. We have used 51 vertical levels in the model starting from the surface to 10 hPa. The geographical data e.g. terrain height, land-use etc. have been interpolated from the USGS (United States Geological Survey, Wang et al., 2014) data at 10 min resolution for the model domain using the geogrid program of the WRF Preprocessing System (WPS). The different options used in this study to parametrize the atmospheric processes are listed in Table 1. The instantaneous model output has been stored every hour and has been used for the analysis. Model simulations are conducted for the period of 29 May to 30 September 2008. The first three days output was discarded as the model spin up.

NCEP Final Analysis (FNL from GFS ds083.2) dataset (<http://rda.ucar.edu/datasets/ds083.2/>) with a spatial resolution of 1°, available every 6 h, has been used to provide the initial and lateral boundary conditions for the meteorological fields. Four Dimensional Data Assimilation (FDDA) has been applied to limit the errors in the simulations of meteorological parameters. The horizontal winds, temperature and water vapor are nudged with a nudging coefficient of 0.0006 at all vertical levels. The time step for the simulations has been set at 120 s, which is 4 times the grid resolution (30 km), so that the CFL stability criterion is not violated.

The anthropogenic emissions of CO, NO_x, SO₂, NMVOCs, PM, BC and OC are from the Hemispheric Transport of Air Pollution (HTAP v2) emission inventory available on a monthly temporal resolution (http://edgar.jrc.ec.europa.eu/htap_v2/index.php?SECURE=123). The HTAP emissions are based upon compilation of regional emission inventories available from US EPA for USA, Environment Canada for Canada, EMEP and TNO for Europe and MICS-

Asia for Asian countries including India. The rest of the world is filled by emissions from EDGAR4.3. The HTAP v2 data are harmonized at a spatial resolution of $0.1^\circ \times 0.1^\circ$ for the years 2008 and 2010. We have utilized the emissions available for the year 2008. The emissions available from different sectors such as energy, industry, residential, ground-transport, ships and agriculture have been combined and then mapped on the WRF-Chem grid. Detailed information on the HTAP inventory used can be found in a recent study (Janssens-Maenhout et al., 2015). An additional simulation has also been conducted using a different regional inventory (INTEX-B) (Zhang et al., 2009) for anthropogenic emissions.

The biomass burning emissions to the model have been provided from the Fire INventory from NCAR (FINN), Version 1 (Wiedinmyer et al., 2011). The biogenic emissions are calculated using the Model of Emissions of Gases and Aerosols from Nature (MEGAN) (Guenther et al., 2006) online based on weather and land use data. The gas phase chemistry is represented by the second generation Regional Acid deposition Model (RADM2) (Stockwell et al., 1990), which includes 63 chemical species participating in 21 photolysis and 136 gas phase reactions. The aerosol module is based on the Modal Aerosol Dynamics Model for Europe (MADE) (Binkowski and Shankar, 1995; Ackermann et al., 1998) and Secondary Organic Aerosol Model (SORGAM) (Schell et al., 2001). GOCART dust emissions have been included with AFWA modifications. The feedback from aerosols to the radiation scheme has been turned on in the simulations.

Results from two different MOZART simulations (MOZART-4/NCEP and MOZART-4/GEOS5) were available to use for the initial and boundary conditions for chemical fields in WRF-Chem (<http://www.acd.ucar.edu/wrf-chem/mozart.shtml>). MOZART-4/NCEP simulations are driven by NCEP/NCAR reanalysis meteorological dataset and utilizes emissions based on POET, REAS and GFED2 (Emmons et al., 2010). The spatial resolution of these simulations is $2.8^\circ \times 2.8^\circ$ and has 28 pressure levels from the surface to about 3 hPa. MOZART-4/GEOS-5 simulations are driven by meteorological fields from the NASA GMAO GEOS-5 model. This simulation utilizes the emissions based on inventory by D. Streets for ARCTAS (<http://cgrer.uiowa.edu/arctas>) and fire emissions from FINN-v1 (Wiedinmyer et al., 2011). The spatial resolution of MOZART-4/GEOS5 simulations is $1.9^\circ \times 2.5^\circ$ and

has 56 pressure levels from the surface to about 2 hPa. In this study we show the simulations driven by MOZART-4/GEOS5 initial and boundary conditions. A sensitivity analysis (not shown here) using MOZART4/NCEP data revealed similar results for WRF-Chem simulated free tropospheric ozone and carbon monoxide.

We have conducted four different WRF-Chem simulations by varying the initial and boundary conditions and the anthropogenic emissions as mentioned in Table 2. The first simulation called as “Std” is the standard run without any adjustments in the anthropogenic emissions or MOZART-4/GEOS5 boundary conditions data (Sect. 4.1.1). Std_INTEX is similar to Std run, except that anthropogenic emissions are used from a different inventory (INTEX-B). The additional simulation 1.5×_EM has been conducted by enhancing the anthropogenic emissions over South Asia by a factor of 1.5 to investigate the influence of regional emissions (Sect. 4.2). The simulation 1.25×_BDY has been conducted by enhancing the CO mixing ratios by a factor of 1.25 on the MOZART boundary conditions data at the western fringe of the domain (Sect. 4.3) to study the effect of long-range transport.

2.2 Backward trajectories

In order to investigate the transport of CO over Chennai (Sect. 4.3), 10 day backward air trajectories are simulated using the Hybrid Single Particle Lagrangian Integrated Trajectory (HYSPLIT) model (http://www.arl.noaa.gov/HYSPLIT_info.php). The meteorological inputs to the model are provided from the NCEP/NCAR reanalysis data available every 6 h at a spatial resolution of $2.5^{\circ} \times 2.5^{\circ}$. The top of the model was set at 20 km and the isentropic method has been used for the vertical motion. Backward air trajectories are calculated for each CARIBIC observation day at 18:00 and 22:00 GMT at 6 altitude levels (2, 4, 6, 8, 10, and 12 km a.s.l.) to cover the altitude range of the CARIBIC measurements. More details about the HYSPLIT trajectory simulations (Draxler and Hess, 1997, 1998; Draxler et al., 2014) and use of other meteorological datasets as inputs to the HYSPLIT model over the Indian region can be found elsewhere (Ojha et al., 2012; Sarangi et al., 2014).

3 Observational datasets

3.1 CARIBIC

This study primarily utilizes the in situ measurements of ozone and CO vertical profiles collected over Chennai in the southern Indian region as a part of the CARIBIC project. The CARIBIC observatory is deployed on a monthly basis aboard a Lufthansa Airbus A340-600 for a series of two to six long distance flights. The aircraft is fitted with a permanently mounted inlet system which is connected via stainless steel tubing to the CARIBIC instrument container when installed. Parts of the tubing are lined with thin walled PFA tubes to avoid wall effects (Brenninkmeijer et al., 2007). From April to December 2008, the CARIBIC container measured during 32 flights between Frankfurt, Germany and Chennai. Here we use only the 14 flights conducted between June and September 2008 as these months represent the core of the monsoon period over India in this year as discussed by Schuck et al. (2010) and Baker et al. (2011). All 14 flights crossed the western part of the monsoon anticyclone in the upper troposphere over the western coast of India at altitudes of 10–12 km before reaching Chennai at the east coast. More details regarding the flight tracks can be found in Rauthe-Schöch et al. (2015).

CO is measured with a commercial AeroLaser AL 5002 resonance fluorescence UV instrument modified for use onboard the CARIBIC passenger aircraft. Alterations were necessary to optimise the instrument reliability to allow for automated operation over an entire CARIBIC flight sequence lasting several days. The instrument has a precision of better than 2 nmol mol⁻¹ at an integration time of 1 s. For more details, the reader is referred to Scharffe et al. (2012).

The ozone measurements are performed by a fast, commercially available dry chemiluminescence instrument, which at typical ozone mixing ratios between 10 and 100 nmol mol⁻¹ and a measurement frequency of 10 Hz has a precision of better than 1.0 %. The absolute ozone concentration is inferred from a UV-photometer designed in-house which operates at 0.25 Hz and reaches an accuracy of 0.5 nmol mol⁻¹. More technical details can be found in Zahn et al. (2012). Water vapor mixing ratios were measured using a modified two-channel

photo-acoustic diode-laser spectrometer with a precision of 1 ppmv. These measurements were calibrated using the frost-point hygrometer (Zahn et al., 2014).

3.2 Balloon-borne Measurements

WRF-Chem simulations have also been compared with the ozonesonde observations at Delhi (DEL: 77.1° E, 28.3° N), Pune (PUN: 73.85° E, 18.53° N), and Thiruvananthapuram (TVM: 77.0° E, 8.47° N). These ozonesonde observations are conducted by the Indian Meteorological Department (IMD) and are archived at the World Ozone and Ultraviolet Radiation Data Center (WOUDC) (woudc.org).

The ozonesondes apply a modified electrochemical ozone sensor (Shreedharan, 1968). These ozonesondes have also been a part of the JOSIE intercomparison experiment (Smit and Kley, 1998). The ozonesonde observations have been previously used for analysis of long-term changes in tropospheric ozone over India (Saraf and Beig, 2004). Considering the very low temporal frequency of these observations (lack of any profiles over Delhi during the year 2008 (as of CARIBIC) and lack of observations in individual months e.g. in September over Pune; this dataset has been converted to a monsoon time (June-September) climatology for 2006-2009 period around 2008 for comparison with WRF-Chem simulations. Day-to-day variability in model simulated wind speed at different pressure levels has also been evaluated above Chennai against the radiosonde observations available at <http://weather.uwyo.edu/upperair/sounding.html>.

3.3 Satellite data

We also use vertical profiles of CO retrieved from the Measurements of Pollution in the Troposphere (MOPITT) instrument (<https://www2.acd.ucar.edu/mopitt>) for comparison with WRF-Chem simulations. The MOPITT instrument on the EOS-Terra provides the vertical profiles and global distribution of tropospheric CO with the expected precision of 10 % (Pan et al., 1998; Deeter et al., 2003; Yoon et al., 2013). Because MOPITT measures upwelling infrared radiation at 4.7 and 2.4 μm , it can provide data during night and day. Even

though the retrieval sensitivity is generally greater for daytime than for nighttime overpasses (Deeter, 2013), the nighttime retrievals have been updated by using the improved a priori profiles over land (Ho et al., 2005).

We have used the gridded monthly CO retrievals (MOP03JM) version 6 data, available at <http://reverb.echo.nasa.gov/reverb/>. The major updates with this version include corrected geolocation data, use of NASA MERRA reanalysis product for meteorological fields and a priori surface skin temperatures instead of NCEP and updated CO a priori (Deeter, 2013). The Thermal and Near IR (JIR) retrievals have been utilized to have better sensitivity of MOPITT retrievals in the lower free tropospheric altitudes (Worden et al., 2010). Further information on MOPITT CO retrievals (Deeter et al., 2003, 2004a, b) and comparison with measurements (Emmons et al., 2004, 2007) and model simulations can be found elsewhere (Emmons et al., 2010; Yoon and Pozzer, 2014).

3.4 Ground-based measurements

Ground-based measurements of CO used in the study are obtained from Cape Rama (73.8° E, 15.1° N) located at the western coast of India. These measurements contributed to the Global Atmosphere Watch (GAW) programme of the World Meteorological Organization (WMO, http://www.wmo.int/pages/prog/arep/gaw/gaw_home_en.html). The air samples were analyzed using a Gas Chromatograph (GC) and the reported precision of CO measurements is 1 nmol mol⁻¹ (Bhattacharya et al., 2009). The observations conducted during 1993–2010 have been used to calculate the average seasonal cycle of CO at Cape Rama. More details of the measurement site (Tiwari et al., 2011), sample collection and analysis (Bhattacharya et al., 2009), and WDCGG database can be found elsewhere (<http://ds.data.jma.go.jp/gmd/wdcgg/>).

Ground-based measurements of ozone at the rural site Gadanki (79.2° E, 13.5° N) were obtained from the literature (Naja and Lal, 2002; Renuka et al., 2014). These measurements are based upon the UV-absorption technique. The accuracy of these instruments is reported to be ±5 % (Kleinman et al., 1994).

4 Results and discussion

The general features of the monsoon meteorology and dynamics are reasonably reproduced by WRF-Chem. In the supplement (Figure 1), the WRF-Chem simulated average wind pattern at 850 hPa and Outgoing Longwave Radiation (OLR) are shown for July 2008. The typical monsoonal wind pattern bringing in the moist air masses from oceanic regions is successfully captured by WRF-Chem. Latitudinal extent of low OLR values between 70–100 ° E has also been qualitatively reproduced in agreement with the OLR climatology over this region (Mahakur et al., 2013). The biases in WRF OLR as compared to NOAA OLR data are similar to Srinivas et al. (2015), who compared WRF OLR with reanalysis data. Further details of general meteorology, wind patterns and OLR variations over the Indian region during the summer monsoon can be found elsewhere (e.g. Asnani, 2005; Mahakur et al., 2013; Patwardhan et al., 2014). Detailed evaluations of WRF simulated meteorology (Kumar et al., 2012a) and evaluations of convection parameterizations in WRF model during the summer monsoon over India (Mukhopadhyay et al., 2010) have been published previously.

4.1 Model evaluation

In this section, WRF-Chem simulated ozone and carbon monoxide data over Chennai are evaluated against the CARIBIC observations, MOPITT retrievals of CO profiles and the ground-based measurements.

4.1.1 Comparison with CARIBIC profiles

The hourly output of WRF-Chem simulations have been spatially and temporally interpolated along the CARIBIC flight tracks. The observed and model simulated profiles have been averaged into vertical bins of 50 hPa for the comparison analysis. The comparison of O₃ and CO profiles from CARIBIC measurements with standard WRF-Chem simulations (Std) is shown in Fig. 2. Here we only show the profiles collected during the descent of the aircraft as these have complete coverage until about 800 hPa, while the measurements

start from about 600 hPa upwards in the ascending profiles. However for the analysis of model biases, all the ascending and descending profiles have been averaged to calculate the monthly profiles (Fig. 3).

Higher levels of ozone and carbon monoxide occur in the Lower Troposphere (LT: 850–600 hPa) and Upper Troposphere (UT: above 300 hPa), while lower levels in the Middle Troposphere (MT: 600–400 hPa), cause a typical C-shape structure during July. This feature is suggested to be associated with the monsoonal convective uplifting of the lower tropospheric pollution and is captured by WRF-Chem.

Despite the qualitative agreement of the vertical distributions of O_3 and CO, significant differences occur between model and measurements, particularly in lower tropospheric CO. For example, on 19 June the observational CO levels vary from 91.5 ± 3.9 to 104.4 ± 0.6 nmol mol⁻¹ in the LT, whereas WRF-Chem simulated CO levels are significantly lower (75.4 ± 1.0 to 85.8 ± 0.7 nmol mol⁻¹). The average underestimation (Mean Bias) of CO in the LT is found to be 12.6 ± 4.4 , 22.8 ± 12.6 and 19.9 ± 7.5 nmol mol⁻¹ during June, July and August respectively, as calculated from all the ascent and descent profiles averaged for a month (Fig. 3). WRF-Chem simulated average CO shows very good agreement with CARIBIC measurements during September in the LT (MB = -0.1 ± 4.2 nmol mol⁻¹).

The model underestimates a pollution event of strongly elevated ozone observed on 15 July 2008 (146.4 ± 12.8 nmol mol⁻¹ at 810 hPa). In contrast to CO which is typically underestimated in LT, the bias in model simulated O_3 varies from an overestimation by 4.3 ± 1.8 during June to an underestimation by 7.8 ± 1.6 nmol mol⁻¹ during August, except during the strong pollution event (-71.5 ± 25.9 nmol mol⁻¹). The significantly higher levels of O_3 (146.4 ± 12.8 nmol mol⁻¹) and CO (136.4 ± 12.2 nmol mol⁻¹) as observed during July are from two observational profiles on the same day (15 July), discussed separately as an event of strong pollution.

For the complete profiles from Standard WRF-Chem simulations (Std), the Root Mean square Deviation (RMSD) values for O_3 are found to vary from 6.5 to 12.6 nmol mol⁻¹, except during a strong pollution event (RMSD = 48.1 nmol mol⁻¹). RMSD values for CO are in the range of 5.5 to 18.2 nmol mol⁻¹. Additional simulation Std_INTEX using a different

emission inventory INTEX-B also shows similar results (Fig. 3, Supplementary material-Figure 2), as seen with simulation Std using HTAP emissions. The average vertical distribution of the water vapor mixing ratios from WRF-Chem is compared with the CARIBIC measurements in Fig. 4. Generally, WRF-Chem simulated H_2O is in very good agreement with the observations, i.e. within the variability of 1-standard deviation. The observations are not available below 500 hPa in months other than during July, when the model tends to overestimate H_2O in the lower troposphere.

4.1.2 Comparison with Ozonesonde Climatology

WRF-chem simulated ozone profiles are compared with the monsoon-time climatology obtained from ozonesonde observations at Delhi, Pune and Thiruvananthapuram (Fig. 5), as described in subsection 3.2. WRF-Chem simulated ozone profiles in the lower and middle troposphere are generally observed to be within the 1-standard deviation variability of the observational climatology over the three stations. However, in the upper troposphere, WRF-Chem overestimates ozone mixing ratios over Delhi and Pune. The mean biases of the WRF-Chem are estimated against average ozonesonde climatology in summer monsoon in the LT (850–650 hPa) as calculated against CARIBIC observations in Section 4.1.1. MB in the LT are found to be lower at Delhi ($-2.2 \pm 3.8 \text{ nmol mol}^{-1}$) and Pune ($-1.2 \pm 3.6 \text{ nmol mol}^{-1}$), as compared to that over Thiruvananthapuram ($-12.4 \pm 1.3 \text{ nmol mol}^{-1}$). However, in the UT (e.g. at 150 hPa) ozone mixing ratios in WRF-Chem simulations at Delhi ($94.1 \pm 31.1 \text{ nmol mol}^{-1}$) and Pune ($69.4 \pm 23.5 \text{ nmol mol}^{-1}$) are found to be higher as compared to ozonesonde observations (61.1 ± 34.0 and $31.3 \pm 17.5 \text{ nmol mol}^{-1}$ respectively). The overestimation in upper troposphere by WRF-Chem has been reported earlier with a slightly different model setup (different convective parameterization) (Kumar et al., 2012b).

4.1.3 Comparison with MOPITT CO profiles

Figure 6 shows the monthly average CO profiles from simulation Std and the CO retrievals obtained from MOPITT over Chennai. For consistency with the comparison with CARIBIC observations (Sect. 4.1.1), which are collected only during nighttime, we restrict the comparison of WRF-Chem and MOPITT to nighttime data, though we do not find large diel variability in free tropospheric CO in our simulations. The averaging kernel and the a priori profiles of MOPITT data have been applied on the monthly average CO profile from standard WRF-Chem simulation, denoted as Std(AK).

In contrast to the comparison with the in situ vertical profiles from CARIBIC, the WRF-Chem simulated CO shows very good agreement with the satellite data in the lower troposphere during June. The mean bias value between WRF-Chem and MOPITT is found to be $1.5 \pm 0.8 \text{ nmol mol}^{-1}$ in the LT during June as compared to the WRF-Chem and CARIBIC data comparison ($-12.6 \pm 4.4 \text{ nmol mol}^{-1}$). Interestingly, in comparison to the satellite data, WRF-Chem is found to overestimate CO in the LT by 21.4 ± 2.8 , 37.8 ± 5.0 , and $26.9 \pm 4.0 \text{ nmol mol}^{-1}$ during July, August and September respectively. Middle tropospheric CO is also significantly overestimated by WRF-Chem as compared to MOPITT during July–September. This could be partially associated with the unscreened-out cloud contamination in the satellite retrievals during the summer monsoon season. The a priori CO data from the global chemistry transport model could be another potential source of the discrepancy (Asatar and Nair, 2010).

WRF-Chem profiles, after applying the satellite operator become very similar to the satellite a priori, especially in the lower and middle troposphere. During this period, averaging kernels in the lower troposphere are found to be smaller (less than 0.1) as compared to the values reported for example during spring (Kar et al., 2008). This indicates relatively lower sensitivity of MOPITT for lower tropospheric CO over this region during the summer monsoon. The different results regarding the WRF-Chem evaluation against the in situ measurements and satellite data clearly highlight the need of more in situ measurements of vertical profiles for validation of chemistry-transport models as well as the satellite retrievals over

this region, particularly during the monsoon, when the sky is obscured by clouds. Such studies would be invaluable for addressing the discrepancies due to limited overpassing time for MOPITT, retrieval errors due to sensor degradation, not updated CO a priori, cloud-contamination, systematic errors as well as errors in model simulations.

4.1.4 Surface O₃ and CO

In order to understand if the observed discrepancies between WRF-Chem and CARIBIC observations are associated with emissions and processes at the surface in India, we analyze the variations in surface ozone and CO over this region. WRF-Chem (Std) simulated average distributions of surface O₃ and CO over the Indian region are shown in Fig. 7 for the four months of the summer monsoon in 2008. The distribution of O₃ as well as CO shows large spatial heterogeneity across the region in all four months.

Surface ozone levels are typically lower ($< 30 \text{ nmol mol}^{-1}$) than aloft over most of the domain. The ozone levels are found to be highest over the polluted Indo-Gangetic Plain (IGP), in northeastern India, and also over the eastern coastal region ($40\text{--}50 \text{ nmol mol}^{-1}$). Average surface ozone levels over most of the Indian region are relatively low, mostly below 40 nmol mol^{-1} , which is mainly due to the inflow of marine air masses and suppressed photochemistry in cloudy/rainy conditions. The highest levels of surface ozone are simulated over the northern part of the domain, where the influences of marine air/monsoon are relatively smallest. While, vertical trace gas distributions are affected by monsoon convection, both CO and O₃ are not soluble and not directly affected by precipitation scavenging. Wet scavenging of O₃ precursors and prevailing cloudy-rainy meteorological conditions, however, could suppress the ozone production, particularly near the surface. CO mixing ratios vary from about 50 to $300 \text{ nmol mol}^{-1}$, except over the IGP where a high CO belt ($400 \text{ nmol mol}^{-1}$ and more) accumulates throughout the monsoon season. Towards the end of the monsoon period in September, ozone and CO levels show most pronounced enhancements over the IGP and also a tendency of pollution buildup in the surrounding regions.

The WRF-Chem simulated spatial distributions of surface ozone and CO are found to be consistent with previous studies over the Indian region mostly based on satellite observations (Fishman et al., 2003; Kar et al., 2008), simulations with a global chemistry transport model (Ojha et al., 2012) and a previous study evaluating WRF-Chem simulations over the Indian region (Kumar et al., 2012b). WRF-Chem simulations were found to significantly overestimate surface O₃ and underestimate CO at an urban site in the Indo-Gangetic Plain towards the onset of monsoon, while the model was in better agreement during May (Michael et al., 2014).

Figure 8 shows a comparison of surface ozone and CO variations from WRF-Chem with ground-based observations. Unfortunately simultaneous measurements of ozone and CO are sparse over this region and therefore observations of ozone are utilized from Gadanki (79.2° E, 13.5° N), a rural site in southern India (Naja and Lal, 2002; Renuka et al., 2014) and observations of CO are used from the coastal site Cape Rama (73.8° E 15.1° N) (Yoon and Pozzer, 2014). O₃ and CO model results from the Std simulation are found to be within the 1 σ standard deviations of the measurements at Gadanki and Cape Rama.

The significant underestimation of CO by WRF-Chem in the free troposphere (Sect. 4.1.1) as compared to CARIBIC measurements is not evident at the surface. It is suggested that the discrepancies between WRF-Chem and CARIBIC observations are likely not caused directly by surface emissions and chemistry and may be associated with the influence of large-scale air mass transports. We further investigate this by conducting a sensitivity simulation with 50 % higher CO emissions (Sect. 4.2) over the Indian region. The possible role of transport is investigated by backward air trajectory analysis and conducting a sensitivity run with 25 % higher influx of CO from the domain boundary based on trajectories (Sect. 4.3).

4.2 Sensitivity to regional emissions

A sensitivity simulation 1.5 \times _EM has been conducted by enhancing the CO emissions over the entire south Asian domain (Fig. 1) by 50 %, keeping all other inputs fixed as for the Standard WRF-Chem simulations (Std, Table 2). Previous studies (e.g. Randel et al., 2010; Fadnavis et al., 2013, 2015) have shown that monsoonal convection plays a key role

in uplifting the boundary layer emissions / pollution into the Upper Troposphere and Lower Stratosphere (ULTS) altitudes. To investigate this effect, we compare the monthly average horizontal distribution of CO from Std and $1.5\times_EM$ simulations for upper tropospheric altitudes (average for 116 – 211 hPa) (Fig. 9).

5 The spatial distribution of CO in the upper troposphere shows highest levels in the northern and central Indian region in both of the simulations. The effects of the monsoonal circulation are clearly visible through convectively uplifted CO from regional emissions, in particular from the Indo-Gangetic Plain (IGP) towards the west. The sensitivity simulation shows significant influence on the upper tropospheric CO distribution and increases the westward
10 export of pollution. For example, over the north-central Indian region the CO mixing ratios are found to be higher by about 20 % in $1.5\times_EM$ simulation as compared to Std simulation.

The comparison of monthly average CO over Chennai between the standard simulation and $1.5\times_EM$ is shown in Fig. 10. The percentage enhancement in the CO mixing ratios due to the increased emissions is also shown. The maximum impact (33 %) of the increased
15 anthropogenic emissions on CO mixing ratios is observed near the surface. The direct impact of emission enhancement is found to be significantly lower (5 % and less) from 850 hPa and above, where WRF-Chem was found to most strongly underestimate the CO levels.

Hence a significant increase (50 %) in the regional anthropogenic emissions over India led to only minor enhancements in the model CO levels as compared to the observed under-
20 estimation in the lower free troposphere. Furthermore, the WRF-Chem simulated surface CO is in good agreement with ground-based observations over this region. Therefore, it is concluded that the observed underestimation of CO by WRF-Chem in the free troposphere is not primarily associated with local and regional anthropogenic emissions. The next possibility of transport of CO into the domain as controlled by the chemical boundary conditions
25 in WRF-Chem is investigated in the next subsection.

4.3 Influence of transport

We investigate the role of transport over Chennai utilizing the 10 day backward trajectories simulated using the HYSPLIT model in conjunction with a sensitivity simulation with the

MOZART/GEOS5 boundary condition. Air mass trajectories color coded according to the starting altitude over Chennai for all the CARIBIC observation days are shown in Fig. 11. Synoptic wind patterns appear to be very different in the lower troposphere (2–4 km) compared to higher altitudes (8–12 km). Lower tropospheric air over Chennai has been dominantly influenced by westerly air masses, while the upper tropospheric air masses primarily originated from the east during June–August. The wind patterns change significantly towards the end of the monsoon period (September), when the trajectories are influenced by different continental regions of South Asia.

To investigate the transport/influences from local/regional pollution, we calculated the residence time of the air masses and mean pressure along the trajectory over the southern Indian region (74.9 to 81.7° E and 9.9 to 17.1° N) for all the backward air trajectories at 2 and 4 km altitude above Chennai (Fig. 12). Residence time is derived by counting number of hours in the air trajectory within the specified south Indian region and converting it into days. For all days the residence time in South India was about a day, except for 15 July 2008 when the residence time was more than 3 days.

4.3.1 Strong pollution event on 15 July 2008

We begin by examining a pollution event observed on 15 July 2008 over Chennai to investigate its origin. Ozone and carbon monoxide levels were observed to be very high during the month of July but are substantially underestimated by WRF-Chem (Fig. 2 and Fig. 3). Since there were only two observational profiles during July and both on the same day (15 July 2008), this observation is suggested to be more representative of a pollution event rather than the monthly average conditions over this region. During this event, O_3 ($146.4 \pm 12.8 \text{ nmol mol}^{-1}$) and CO ($136.4 \pm 12.2 \text{ nmol mol}^{-1}$) mixing ratios are found to be very high in the lower troposphere ($\sim 805 \text{ hPa}$), indicating that these concentrations are associated with the transport of polluted air with ample time for photochemical ozone build up, while significant influence of transport of ozone rich air from the stratosphere is unlikely. It is found that the residence time of this air mass is more than 3 days over southern India during this event, much longer than during CARIBIC flight times in other months. Moreover, the air

masses are found to be influenced by boundary layer pollution as indicated by significantly higher mean pressure along the trajectory (915 ± 43 hPa). To investigate the underprediction of the event in the model, we analyzed the wind fields over Chennai from radiosonde measurements. The model is found to generally reproduce the variations in wind speed over Chennai at different altitude levels (e.g. in the range of 4-10 m/s at 980 hPa) (Supplementary material- Figure 3, 4). However, the model does not capture the occurrences of low-wind speed (1-3 m/s) and overestimates systematically the wind speed during the July period. Therefore the air parcels could not possibly collect enough pollutants from the boundary layer leading to the underprediction of the strong pollution event in model. Additionally, no indication of underestimation of emissions is found as the model performance did not improve in reproducing the event when emissions were increased by 50%.

4.3.2 Long-range transport

Long-range transport of pollution in regional models is controlled by the chemical boundary conditions, generally provided from a global model. Previous studies investigated the impact (Pfister et al., 2013) and uncertainties (Andersson et al., 2015) in long-range transport in regional model simulations. In WRF-Chem simulations in this study the long-range transport is controlled by the time varying chemical boundary conditions from a global model MOZART/GEOS5 simulations.

We assess the contribution of long-range transport of CO in the lower troposphere over Chennai by conducting a sensitivity simulation with increased CO at the domain boundary. Backward air trajectories suggest that CO is significantly underestimated in the lower troposphere in westerly air masses (Figs. 3 and 11). Therefore, we increase the CO mixing ratios by 25% in the MOZART/GEOS5 data, over a region ($7.5^\circ \text{ N} < \text{lat} < 16.5^\circ \text{ N}$) on the western boundary as shown in Fig. 13, chosen suitably based on the backward trajectories (Fig. 11).

Figure 14 shows a comparison of average CO profiles from CARIBIC measurements, WRF Chem standard simulations (Std) and the sensitivity simulation with increased CO at the western boundary ($1.25 \times \text{BDY}$). In contrast to the sensitivity run with increased

emissions ($1.5 \times \text{EM}$), here we find significant improvement in the WRF-Chem simulated CO in the free troposphere. For example during June, WRF-Chem simulated CO mixing ratios from $1.25 \times \text{BDY}$ simulation ($95.8 \pm 4.3 \text{ nmol mol}^{-1}$) are comparable to the observations ($96.6 \pm 9.1 \text{ nmol mol}^{-1}$) at $\sim 800 \text{ hPa}$. The improvements are also significant in other months in the lower free troposphere. In contrast to the June–August period, the air masses over Chennai show influences of higher emissions on the free troposphere. This could be associated with the transport from the continental Indian region as shown by backward trajectories (Fig. 11). The enhancements due to higher CO in the boundary conditions are significantly less during September as compared to June–August. We suggest that since air masses over Chennai during September are more influenced by the regional emissions, the influence of uncertainty in boundary conditions is not evident here. Further it is noted that such dominance of regional impacts on CO vertical distributions during September is captured better by WRF-Chem, as compared to the global model simulation (Supplement Fig. 5).

This study suggests that anticyclonic advection plays a very important role which could transport polluted air masses from outside the region (domain) during the summer monsoon. This complements conventional thinking that convected regional emissions dominate the tropospheric composition during the monsoon season and points to a potentially significant external source of pollution to the monsoon anticyclone. We show that this transport is generally very fast i.e. the residence time of air masses is 1–2 days over southern India, except during the strong pollution event (Sect. 4.3.1). This rapid transport could advect CO-rich air masses from more strongly polluted upwind regions. As indicated by the backward air trajectories and a sensitivity run, CO-rich air masses could originate in central Africa and the Persian Gulf region. During the summer monsoon, CO mixing ratios have been found to be highest over central Africa associated with biomass burning emissions (Torres et al., 2010; Inness et al., 2013, and references therein). A recent study utilizing the trajectory-mapping technique and aircraft observations (Osman et al., 2015) also indicated elevated CO mixing ratios over the western boundary of our model domain. We suggest that improvements in the global fire emissions input to the global models and data assimilation

lation would be helpful in better constraining the effects of long-range transport during the monsoon. Regional emissions from continental India are shown to significantly influence the free troposphere over Southern India towards the end of the monsoon (September).

5 Conclusions

In this paper we integrated the aircraft-borne measurements of O_3 and CO vertical profiles collected as a part of the CARIBIC program with WRF-Chem simulations over India for the summer monsoon period in the year 2008. Evaluation of the model results against in situ O_3 and CO profiles revealed the capabilities as well as limitations of the WRF-Chem simulations over this region. The WRF-Chem simulated spatial distribution of ozone and CO at the surface is largely consistent with previous studies over this region based on satellite-based measurements and model simulations. WRF-Chem simulated ozone profiles were in good agreement with ozonesonde climatology over Delhi and Pune in the lower to middle troposphere, while negative bias was found over Thiruvananthapuram. CARIBIC observations over Chennai show higher levels in the lower and upper troposphere and lower levels in the middle troposphere causing a typical C-shape profile in the O_3 and CO distributions. This feature has been observed to be most pronounced during July and has been qualitatively captured by WRF-Chem.

The major limitation of the model is found to be underestimation ($12.6\text{--}22.8\text{ nmol mol}^{-1}$) of CO in the lower free troposphere during June to August. Model simulated CO is in very good agreement with CARIBIC measurements during September. The model biases in lower tropospheric O_3 are found to vary from an overestimation by about 4.3 nmol mol^{-1} (June) to an underestimation by 7.8 nmol mol^{-1} (August). Additional simulations using a different emission inventory (INTEX-B) showed similar results. WRF-Chem simulated CO is also compared with satellite (MOPITT) retrievals. Interestingly, WRF-Chem is found to overestimate CO compared to MOPITT data during July–September, while, WRF-Chem and MOPITT CO are in very good agreement during June. The contrasting evaluation results of WRF-Chem with in situ measurements and satellite retrievals points towards a need

of more measurements to validate the satellite data and evaluate model results over this region.

WRF-Chem simulations are also compared with the ground-based measurements of ozone and CO at Gadanki (79.2° E, 13.5° N) and Cape Rama (73.8° E, 15.1° N). It is shown that the model simulated O₃ as well as CO at the surface is within the observed variabilities (1 σ). This indicates that the discrepancy between the WRF-Chem simulated and CARIBIC measured CO is likely not directly associated with the regional surface emissions. This is corroborated by a sensitivity simulation with 50 % higher CO emissions over India which leads to about 33 % enhancement at the surface but small influence (5 %) above 850 hPa. Nevertheless, the increase in regional emissions of CO was found to influence the upper tropospheric distribution over north and central Indian region, increasing westward export by about 20%.

Analysis of backward airmass trajectories and wind speed data from model and radiosonde observations over Chennai suggested that a strong pollution event observed during July (O₃: 146.4 ± 12.8 nmol mol⁻¹, CO: 136.4 ± 12.2 nmol mol⁻¹) was associated with stagnation of regional photochemically-processed air mass over southern India.

We find that the lower free troposphere over this region is strongly influenced by air masses from the west during the summer monsoon. A sensitivity simulation with 25 % higher CO mixing ratios over a region at the western boundary of the domain, chosen suitably based on back air trajectories, shows significant improvement in the computed CO levels. We suggest that long-range transport of CO over southern India, originated in Africa, is underestimated in model simulations during the summer monsoon and may have a significant impact on the regional CO budget. We recommend improvement of the global fire emissions and data assimilation in the global models to better constrain long-range transport in WRF-Chem. The effects of regional emissions and synoptic-scale transport over south Asia are better captured by the WRF-Chem. Therefore, improved boundary conditions data combined with regional model will be suitable for chemical budget studies. Additionally, the aircraft-based measurements of trace gases should be supplemented with collocated measurements relevant for the evaluation of parameterization schemes particu-

larly of convection (e.g. Mukhopadhyay et al., 2010) and boundary layer processes during the monsoon which must be simulated correctly in the model to reproduce the tracer transport. Our study highlights that in situ measurements limited only to the ground are insufficient to understand the transport of trace gases, and that aircraft-borne measurements of ozone precursors are essential to improve the model simulations and the understanding of regional tropospheric chemistry.

**The Supplement related to this article is available online at
doi:10.5194/acpd-0-1-2016-supplement.**

Acknowledgements. We thank CARIBIC partners as well as Lufthansa, especially T. Dauer and A. Waibel, and Lufthansa Technik for support. We especially acknowledge D. Scharffe, C. Koeppel and S. Weber for the operation of CARIBIC. The HTAP v2 anthropogenic emissions were obtained from http://edgar.jrc.ec.europa.eu/htap_v2/index.php?SECURE=123. Initial and boundary conditions data for meteorological fields have been obtained from <http://rda.ucar.edu/datasets/ds083.2/>. MOZART-4/NCEP and MOZART-4/GEOS5 initial and boundary condition data for chemical fields, biogenic emissions, biomass-burning emissions and programs to process these datasets were obtained from NCAR Atmospheric Chemistry Division website (<http://www.acd.ucar.edu/wrf-chem/>). We acknowledge NASA Reverb (<http://reverb.echo.nasa.gov/reverb/>) for providing MOPITT CO version 6 data. We acknowledge the World Data Centre for Greenhouse Gases (WDCGG, <http://ds.data.jma.go.jp/gmd/wdcgg/>) for surface CO data. The authors acknowledge the NOAA Air Resources Laboratory (ARL) for the HYSPLIT transport and dispersion model. The WRF-Chem simulations have been performed on the supercomputer HYDRA (<http://www.rzg.mpg.de/>). N. Ojha is thankful to Martin Körfer and Rüdiger Sörensen for their help with computing and data storage. Ozone-sonde observations conducted by Indian Meteorological Department (IMD) were obtained from the WOUDC database. Radiosonde observations of wind speeds were obtained from University of Wyoming website. Use of INTEX-B emission inventory is highly acknowledged. The constructive comments and suggestions from three anonymous reviewers are greatly appreciated.

The article processing charges for this open-access publication were covered by the Max Planck Society.

References

- Ackermann, I. J., Hass, H., Memmesheimer, M., Ebel, A., Binkowski, F. S., and Shankar, U.: Modal aerosol dynamics model for Europe: development and first applications, *Atmos. Environ.*, 32, 2981–2999, doi:10.1016/S1352-2310(98)00006-5, 1998.
- 5 Akimoto, H.: Global air quality and pollution, *Science*, 302, 1716–1719, doi:10.1126/science.1092666, 2003.
- Andersson, E., Kahnert, M., and Devasthale, A.: Methodology for evaluating lateral boundary conditions in the regional chemical transport model MATCH (v5.5.0) using combined satellite and ground-based observations, *Geosci. Model Dev.*, 8, 3747–3763, doi:10.5194/gmd-8-3747-2015, 10 2015.
- Asatar, G. I. and Nair, P. R.: Spatial distribution of near-surface CO over bay of Bengal during winter: role of transport, *J. Atmos. Sol.-Terr. Phys.*, 72, 1241–1250, doi:10.1016/j.jastp.2010.07.025, 2010.
- Asnani, G. C.: *Climatology of the tropics*, in: *Tropical Meteorology*, Vol. 1, 100–204, 2005
- Baker, A. K., Schuck, T. J., Slemr, F., van Velthoven, P., Zahn, A., and Brenninkmeijer, C. A. M.: 15 Characterization of non-methane hydrocarbons in Asian summer monsoon outflow observed by the CARIBIC aircraft, *Atmos. Chem. Phys.*, 11, 503–518, doi:10.5194/acp-11-503-2011, 2011.
- Beig, G. and Brasseur, G. P.: Influence of anthropogenic emissions on tropospheric ozone and its precursors over the Indian tropical region during a monsoon, *Geophys. Res. Lett.*, 33, L07808, doi:10.1029/2005GL024949, 2006.
- 20 Bhattacharya, S. K., Borole, D. V., Francey, R. J., Allison, C. E., Steele, L. P., Krummel, P., Langenfelds, R., Masarie, K. A., Tiwari, Y. K., and Patra, P. K.: Trace gases and CO₂ isotope records from Cabo de Rama, India, *Curr. Sci. India*, 97, 1336–1344, 2009.
- Binkowski, F. S. and Shankar, U.: The regional particulate matter model: 1. Model description and preliminary results, *J. Geophys. Res.-Atmos.*, 100, 26191–26209, doi:10.1029/95JD02093, 1995.
- 25 Brenninkmeijer, C. A. M., Crutzen, P., Boumard, F., Dauer, T., Dix, B., Ebinghaus, R., Filippi, D., Fischer, H., Franke, H., Frieß, U., Heintzenberg, J., Helleis, F., Hermann, M., Kock, H. H., Koepfel, C., Lelieveld, J., Leuenberger, M., Martinsson, B. G., Miemczyk, S., Moret, H. P., Nguyen, H. N., Nyfeler, P., Oram, D., O'Sullivan, D., Penkett, S., Platt, U., Pupek, M., Ramonet, M., Randa, B., Reichelt, M., Rhee, T. S., Rohwer, J., Rosenfeld, K., Scharffe, D., Schlager, H., Schumann, U., 30 Slemr, F., Sprung, D., Stock, P., Thaler, R., Valentino, F., van Velthoven, P., Waibel, A., Wandel, A., Waschitschek, K., Wiedensohler, A., Xueref-Remy, I., Zahn, A., Zech, U., and Ziereis, H.: Civil Aircraft for the regular investigation of the atmosphere based on an instrumented container:

The new CARIBIC system, *Atmos. Chem. Phys.*, 7, 4953–4976, doi:10.5194/acp-7-4953-2007, 2007.

Chen, F. and Dudhia, J.: Coupling and advanced land surface-hydrology model with the Penn State-NCAR MM5 modeling system, Part I: Model implementation and sensitivity, *Mon. Weather Rev.*, 129, 569–585, 2001.

Chou, M.-D. and Suarez, M. J.: An efficient thermal infrared radiation parametrization for use in general circulation models, *NASA Tech. Memo.*, 104606, 85 pp., 1994.

Cristofanelli, P., Putero, D., Adhikary, B., Landi, T. C., Marinoni, A., Duchi, R., Calzolari, F., Laj, P., Stocchi, P., Verza, G., Vuillermoz, E., Kang, S., Ming, J., and Bonasoni, P.: Transport of short-lived climate forcers/pollutants (SLCF/P) to the Himalayas during the South Asian summer monsoon onset, *Environ. Res. Lett.*, 9, 084005, doi:10.1088/1748-9326/9/8/084005, 2014.

David, L. M. and Nair, P. R.: Diurnal and seasonal variability of surface ozone and NO_x at a tropical coastal site: association with mesoscale and synoptic meteorological conditions, *J. Geophys. Res.-Atmos.*, 116, D10303, doi:10.1029/2010JD015076, 2011.

Deeter, M. N.: MOPITT (Measurements of Pollution in the Troposphere): Version 6 Product User's Guide, available at: http://www.acom.ucar.edu/mopitt/v6_users_guide_beta.pdf (last access: 4 August 2015), 2013.

Deeter, M. N., Emmons, L. K., Francis, G. L., Edwards, D. P., Gille, J. C., Warner, J. X., Khattatov, B., Ziskin, D., Lamarque, J.-F., Ho, S.-P., Yudin, V., Attié, J.-L., Packman, D., Chen, J., Mao, D., and Drummond, J. R.: Operational carbon monoxide retrieval algorithm and selected results for the MOPITT instrument, *J. Geophys. Res.-Atmos.*, 108, 4399, doi:10.1029/2002JD003186, 2003.

Deeter, M. N., Emmons, L. K., Edwards, D. P., Gille, J. C., and Drummond, J. R.: Vertical resolution and information content of CO profiles retrieved by MOPITT, *Geophys. Res. Lett.*, 31, L15112, doi:10.1029/2004GL020235, 2004a.

Deeter, M. N., Emmons, L. K., Francis, G. L., Edwards, D. P., Gille, J. C., Warner, J. X., Khattatov, B., Ziskin, D., Lamarque, J.-F., Ho, S.-P., Yudin, V., Attié, J.-L., Packman, D., Chen, J., Mao, D., Drummond, J. R., Novelli, P., and Sachse, G.: Evaluation of operational radiances for the Measurements of Pollution in the Troposphere (MOPITT) instrument CO thermal band channels, *J. Geophys. Res.-Atmos.*, 109, D03308, doi:10.1029/2003JD003970, 2004b.

Draxler, R. and Hess, G.: Description of the HYSPLIT 4 modeling system, *NOAA Tech. Memo. ERL ARL-224*, NOAA Air Resources Laboratory, Silver Spring, MD, 24 pp., 1997.

Draxler, R. and Hess, G.: An overview of the HYSPLIT 4 modeling system of trajectories, dispersion, and deposition, *Aust. Meteorol. Mag.*, 47, 295–308, 1998.

Draxler, R., Stunder, B., Rolph, G., Stein, A., and Taylor, A.: HYSPLIT4 USER's GUIDE, available at: http://www.arl.noaa.gov/documents/reports/hysplit_user_guide.pdf (last access: 4 August 2015), 2014.

Emmons, L. K., Deeter, M. N., Gille, J. C., Edwards, D. P., Attié, J.-L., Warner, J., Ziskin, D., Francis, G., Khattatov, B., Yudin, V., Lamarque, J.-F., Ho, S.-P., Mao, D., Chen, J. S., Drummond, J., Novelli, P., Sachse, G., Coffey, M. T., Hannigan, J. W., Gerbig, C., Kawakami, S., Kondo, Y., Takegawa, N., Schlager, H., Baehr, J., and Ziereis, H.: Validation of Measurements of Pollution in the Troposphere (MOPITT) CO retrievals with aircraft in situ profiles, *J. Geophys. Res.-Atmos.*, 109, D03309, doi:10.1029/2003JD004101, 2004.

Emmons, L. K., Pfister, G. G., Edwards, D. P., Gille, J. C., Sachse, G., Blake, D., Wofsy, S., Gerbig, C., Matross, D., and Nédélec, P.: Measurements of Pollution in the Troposphere (MOPITT) validation exercises during summer 2004 field campaigns over North America, *J. Geophys. Res.-Atmos.*, 112, D12S02, doi:10.1029/2006JD007833, 2007.

Emmons, L. K., Walters, S., Hess, P. G., Lamarque, J.-F., Pfister, G. G., Fillmore, D., Granier, C., Guenther, A., Kinnison, D., Laepple, T., Orlando, J., Tie, X., Tyndall, G., Wiedinmyer, C., Baughcum, S. L., and Kloster, S.: Description and evaluation of the Model for Ozone and Related chemical Tracers, version 4 (MOZART-4), *Geosci. Model Dev.*, 3, 43–67, doi:10.5194/gmd-3-43-2010, 2010.

Fadnavis, S., Semeniuk, K., Pozzoli, L., Schultz, M. G., Ghude, S. D., Das, S., and Kakatkar, R.: Transport of aerosols into the UTLS and their impact on the Asian monsoon region as seen in a global model simulation, *Atmos. Chem. Phys.*, 13, 8771–8786, doi:10.5194/acp-13-8771-2013, 2013.

Fadnavis, S., Semeniuk, K., Schultz, M. G., Kiefer, M., Mahajan, A., Pozzoli, L., Sonbawane, S.: Transport pathways of peroxyacetyl nitrate in the upper troposphere and lower stratosphere from different monsoon systems during the summer monsoon season, *Atmos. Chem. Phys.*, 15, 11477–11499, doi:10.5194/acp-15-11477-2015, 2015.

Fishman, J., Wozniak, A. E., and Creilson, J. K.: Global distribution of tropospheric ozone from satellite measurements using the empirically corrected tropospheric ozone residual technique: Identification of the regional aspects of air pollution, *Atmos. Chem. Phys.*, 3, 893–907, doi:10.5194/acp-3-893-2003, 2003.

Ghude, S. D., Jena, C., Chate, D. M., Beig, G., Pfister, G. G., Kumar, R., and Ramanathan, V.: Reductions in India's crop yield due to ozone, *Geophys. Res. Lett.*, 41, 5685–5691, doi:10.1002/2014GL060930, 2014.

Grell, G. A., Peckham, S. E., Schmitz, R., McKeen, S. A., Frost, G., Skamarock, W. C., and Eder, B.: Fully coupled “online” chemistry within the WRF model, *Atmos. Environ.*, 39, 6957–6975, doi:10.1016/j.atmosenv.2005.04.027, 2005.

5 Guenther, A., Karl, T., Harley, P., Wiedinmyer, C., Palmer, P. I., and Geron, C.: Estimates of global terrestrial isoprene emissions using MEGAN (Model of Emissions of Gases and Aerosols from Nature), *Atmos. Chem. Phys.*, 6, 3181–3210, doi:10.5194/acp-6-3181-2006, 2006.

Ho, S.-P., Edwards, D. P., Gille, J. C., Chen, J., Ziskin, D., Francis, G. L., Deeter, M. N., and Drummond, J. R.: Estimates of 4.7 μm surface emissivity and their impact on the retrieval of tropospheric carbon monoxide by Measurements of Pollution in the Troposphere (MOPITT), *J. Geophys. Res.-Atmos.*, 110, D21308, doi:10.1029/2005JD005946, 2005.

10 Inness, A., Baier, F., Benedetti, A., Bouarar, I., Chabrillat, S., Clark, H., Clerbaux, C., Coheur, P., Engelen, R. J., Errera, Q., Flemming, J., George, M., Granier, C., Hadji-Lazaro, J., Huijnen, V., Hurtmans, D., Jones, L., Kaiser, J. W., Kapsomenakis, J., Lefever, K., Leitão, J., Razinger, M., Richter, A., Schultz, M. G., Simmons, A. J., Suttie, M., Stein, O., Thépaut, J.-N., Thouret, V., Vrekoussis, M., Zerefos, C., and the MACC team: The MACC reanalysis: an 8 yr data set of atmospheric composition, *Atmos. Chem. Phys.*, 13, 4073–4109, doi:10.5194/acp-13-4073-2013, 2013.

Janjic, Z. I.: The surface layer in the NCEP Eta Model, Eleventh Conference on Numerical Weather Prediction, Norfolk, VA, 19–23 August, Amer. Meteor. Soc., Boston, Boston, MA, 354–355, 1996.

20 Janjic, Z. I.: Nonsingular Implementation of the Mellor-Yamada Level 2.5 Scheme in the NCEP Meso Model, NCEP Office Note, 437, 61 pp., 2002.

Janssens-Maenhout, G., Crippa, M., Guizzardi, D., Dentener, F., Muntean, M., Pouliot, G., Keating, T., Zhang, Q., Kurokawa, J., Wankmüller, R., Denier van der Gon, H., Klimont, Z., Frost, G., Darras, S., and Koffi, B.: HTAP_v2: a mosaic of regional and global emission gridmaps for 2008 and 2010 to study hemispheric transport of air pollution, *Atmos. Chem. Phys. Discuss.*, 15, 12867–12909, doi:10.5194/acpd-15-12867-2015, 2015.

25 Kar, J., Jones, D. B. A., Drummond, J. R., Attié, J. L., Liu, J., Zou, J., Nichitiu, F., Seymour, M. D., Edwards, D. P., Deeter, M. N., Gille, J. C., and Richter, A.: Measurement of low-altitude CO over the Indian subcontinent by MOPITT, *J. Geophys. Res.-Atmos.*, 113, D16307, doi:10.1029/2007JD009362, 2008.

30 Kleinman, L., Lee, Y.-N., Springston, S. R., Nunnermacker, L., Zhou, X., Brown, R., Hallock, K., Klotz, P., Leahy, D., Lee, J. H., and Newman, L.: Ozone formation at a rural site in the southeastern United States, *J. Geophys. Res.-Atmos.*, 99, 3469–3482, doi:10.1029/93JD02991, 1994.

Kumar, R., Naja, M., Pfister, G. G., Barth, M. C., and Brasseur, G. P.: Simulations over South Asia using the Weather Research and Forecasting model with Chemistry (WRF-Chem): set-up and meteorological evaluation, *Geosci. Model Dev.*, 5, 321–343, doi:10.5194/gmd-5-321-2012, 2012.

5 Kumar, R., Naja, M., Pfister, G. G., Barth, M. C., Wiedinmyer, C., and Brasseur, G. P.: Simulations over South Asia using the Weather Research and Forecasting model with Chemistry (WRF-Chem): chemistry evaluation and initial results, *Geosci. Model Dev.*, 5, 619–648, doi:10.5194/gmd-5-619-2012, 2012.

Kumar, R., Naja, M., Pfister, G. G., Barth, M. C., and Brasseur, G. P.: Source attribution of carbon monoxide in India and surrounding regions during wintertime, *J. Geophys. Res.-Atmos.*, 118, 1981–1995, doi:10.1002/jgrd.50134, 2013.

10 Lal, S. and Lawrence, M. G.: Elevated mixing ratios of surface ozone over the Arabian Sea, *Geophys. Res. Lett.*, 28, 1487–1490, doi:10.1029/2000GL011828, 2001.

Lal, S., Naja, M., and Subbaraya, B.: Seasonal variations in surface ozone and its precursors over an urban site in India, *Atmos. Environ.*, 34, 2713–2724, doi:10.1016/S1352-2310(99)00510-5, 2000.

15 Lal, S., Venkataramani, S., Srivastava, S., Gupta, S., Mallik, C., Naja, M., Sarangi, T., Acharya, Y. B., and Liu, X.: Transport effects on the vertical distribution of tropospheric ozone over the tropical marine regions surrounding India, *J. Geophys. Res.-Atmos.*, 118, 1513–1524, doi:10.1002/jgrd.50180, 2013.

20 Lal, S., Venkataramani, S., Chandra, N., Cooper, O. R., Brioude, J., and Naja, M.: Transport effects on the vertical distribution of tropospheric ozone over western India, *J. Geophys. Res.-Atmos.*, 119, 10012–10026, doi:10.1002/2014JD021854, 2014.

Lawrence, M. G. and Lelieveld, J.: Atmospheric pollutant outflow from southern Asia: a review, *Atmos. Chem. Phys.*, 10, 11017–11096, doi:10.5194/acp-10-11017-2010, 2010.

25 Lawrence, M. G., Rasch, P. J., von Kuhlmann, R., Williams, J., Fischer, H., de Reus, M., Lelieveld, J., Crutzen, P. J., Schultz, M., Stier, P., Huntrieser, H., Heland, J., Stohl, A., Forster, C., Elbern, H., Jakobs, H., and Dickerson, R. R.: Global chemical weather forecasts for field campaign planning: predictions and observations of large-scale features during MINOS, CONTRACE, and INDOEX, *Atmos. Chem. Phys.*, 3, 267–289, doi:10.5194/acp-3-267-2003, 2003.

30 Lelieveld, J., Crutzen, P. J., Ramanathan, V., Andreae, M. O., Brenninkmeijer, C. A. M., Campos, T., Cass, G. R., Dickerson, R. R., Fischer, H., de Gouw, J. A., Hansel, A., Jefferson, A., Kley, D., de Laat, A. T. J., Lal, S., Lawrence, M. G., Lobert, J. M., Mayol-Bracero, O. L., Mitra, A. P., Novakov, T., Oltmans, S. J., Prather, K. A., Reiner, T., Rodhe, H., Scheeren, H. A., Sikka, D., and

- Williams, J.: The Indian Ocean experiment: widespread air pollution from South and Southeast Asia, *Science*, 291, 1031–1036, doi:10.1126/science.1057103, 2001.
- Lelieveld, J., Berresheim, H., Borrmann, S., Crutzen, P. J., Dentener, F. J., Fischer, H., Feichter, J., Flatau, P. J., Heland, J., Holzinger, R., Kormann, R., Lawrence, M. G., Levin, Z., Markowicz, K. M.,
5 Mihalopoulos, N., Minikin, A., Ramanathan, V., de Reus, M., Roelofs, G. J., Scheeren, H. A., Sciare, J., Schlager, H., Schultz, M., Siegmund, P., Steil, B., Stephanou, E. G., Stier, P., Traub, M., Warneke, C., Williams, J., and Ziereis, H.: Global air pollution crossroads over the Mediterranean, *Science*, 298, 794–799, doi:10.1126/science.1075457, 2002.
- Lelieveld, J., Barlas, C., Giannadaki, D., and Pozzer, A.: Model calculated global, regional
10 and megacity premature mortality due to air pollution, *Atmos. Chem. Phys.*, 13, 7023–7037, doi:10.5194/acp-13-7023-2013, 2013.
- Mahakur, M., Prabhu, A., Sharma, A. K., Rao, V. R., Senroy, S., Singh, R., and Goswami, B. N.: A high-resolution outgoing longwave radiation dataset from Kalpana-1 satellite during 2004–2012, *Curr. Sci.*, 105, NO. 8, 2013.
- 15 Mallik, C., Lal, S., Venkataramani, S., Naja, M., and Ojha, N.: Variability in ozone and its precursors over the Bay of Bengal during post monsoon: Transport and emission effects, *J. Geophys. Res.-Atmos.*, 118, 10190–10209, doi:10.1002/jgrd.50764, 2013.
- Michael, M., Yadav, A., Tripathi, S. N., Kanawade, V. P., Gaur, A., Sadavarte, P., and Venkataraman, C.: Simulation of trace gases and aerosols over the Indian domain: evaluation of the WRF-
20 Chem model, *Geosci. Model Dev. Discuss.*, 7, 431–482, doi:10.5194/gmdd-7-431-2014, 2014.
- Mlawer, E. J., Taubman, S. J., Brown, P. D., Iacono, M. J., and Clough, S. A.: Radiative transfer for inhomogeneous atmospheres: RRTM, a validated correlated-k model for the longwave, *J. Geophys. Res.-Atmos.*, 102, 16663–16682, doi:10.1029/97JD00237, 1997.
- 25 Monks, P. S., Archibald, A. T., Colette, A., Cooper, O., Coyle, M., Derwent, R., Fowler, D., Granier, C., Law, K. S., Stevenson, D. S., Tarasova, O., Thouret, V., von Schneidmesser, E., Sommariva, R., Wild, O., and Williams, M. L.: Tropospheric ozone and its precursors from the urban to the global scale from air quality to short-lived climate forcer, *Atmos. Chem. Phys. Discuss.*, 14, 32709–32933, doi:10.5194/acpd-14-32709-2014, 2014.
- Mukhopadhyay, P., Taraphdar, S., Goswami, B. N. and Krishnakumar, K.: Indian Summer Monsoon Precipitation Climatology in a High-Resolution Regional Climate Model: Impacts of Convective Parameterization on Systematic Biases, Weather and Forecasting, 25, 369–387, doi: 10.1175/2009WAF222320.1, 2010.
- 30

- Naja, M. and Lal, S.: Surface ozone and precursor gases at Gadanki (13.5° N, 79.2° E), a tropical rural site in India, *J. Geophys. Res.-Atmos.*, 107, ACH8.1–ACH8.13, doi:10.1029/2001JD000357, 2002.
- Ohara, T., Akimoto, H., Kurokawa, J., Horii, N., Yamaji, K., Yan, X., and Hayasaka, T.: An Asian emission inventory of anthropogenic emission sources for the period 1980–2020, *Atmos. Chem. Phys.*, 7, 4419–4444, doi:10.5194/acp-7-4419-2007, 2007.
- Ojha, N., Naja, M., Singh, K. P., Sarangi, T., Kumar, R., Lal, S., Lawrence, M. G., Butler, T. M., and Chandola, H. C.: Variabilities in ozone at a semi-urban site in the Indo-Gangetic Plain region: association with the meteorology and regional processes, *J. Geophys. Res.-Atmos.*, 117, D20301, doi:10.1029/2012JD017716, 2012.
- Ojha, N., Naja, M., Sarangi, T., Kumar, R., Bhardwaj, P., Lal, S., Venkataramani, S., Sagar, R., Kumar, A., and Chandola, H.: On the processes influencing the vertical distribution of ozone over the central Himalayas: analysis of yearlong ozonesonde observations, *Atmos. Environ.*, 88, 201–211, doi:10.1016/j.atmosenv.2014.01.031, 2014.
- Osman, M., Tarasick, D. W., Liu, J., Moeini, O., Thouret, V., Fioletov, V. E., Parrington, M., Nédélec, P.: Carbon monoxide climatology derived from the trajectory mapping of global MOZAIC-IAGOS data, *Atmos. Chem. Phys.*, 15, 29871–29937, doi:10.5194/acpd-15-29871-2015, 2015
- Pan, L., Gille, J. C., Edwards, D. P., Bailey, P. L., and Rodgers, C. D.: Retrieval of tropospheric carbon monoxide for the MOPITT experiment, *J. Geophys. Res.-Atmos.*, 103, 32277–32290, doi:10.1029/98JD01828, 1998.
- Park, M., Randel, W. J., Gettelman, A., Massie, S. T., and Jiang, J. H.: Transport above the Asian summer monsoon anticyclone inferred from Aura Microwave Limb Sounder tracers, *J. Geophys. Res.-Atmos.*, 112, D16309, doi:10.1029/2006JD008294, 2007.
- Park, M., Randel, W. J., Emmons, L. K., and Livesey, N. J.: Transport pathways of carbon monoxide in the Asian summer monsoon diagnosed from Model of Ozone and Related Tracers (MOZART), *J. Geophys. Res.-Atmos.*, 114, D08303, doi:10.1029/2008JD010621, 2009.
- Patwardhan, S., Kulkarni, A., and Krishna Kumar, K.: Impact of climate change on the characteristics of Indian summer monsoon onset, *Int. J. Atmos. Sci.*, VOL 2014, 201695, doi:10.1155/2014/201695, 2014.
- Pfister, G., G., Walters, S., Emmons, L., K., Edwards, D., P., and Avise, J.: Quantifying the contribution of inflow on surface ozone over California during summer 2008, *J. Geophys. Res. Atmos.*, 118, 12282–12299, doi:10.1002/2013JD020336, 2013.

- Pozzer, A., Zimmermann, P., Doering, U.M., van Aardenne, J., Tost, H., Dentener, F., Janssens-Maenhout, G., and Lelieveld, J.: Effects of business-as-usual anthropogenic emissions on air quality, *Atmos. Chem. Phys.*, 12, 6915–6937, doi:10.5194/acp-12-6915-2012, 2012.
- 5 Pozzer, A., de Meij, A., Yoon, J., Tost, H., Georgoulas, A. K., and Astitha, M.: AOD trends during 2001–2010 from observations and model simulations, *Atmos. Chem. Phys.*, 15, 5521–5535, doi:10.5194/acp-15-5521-2015, 2015.
- Randel, W. J., Park, M., Emmons, L., Kinnison, D., Bernath, P., Walker, K. A., Boone, C., and Pumphrey, H.: Asian monsoon transport of pollution to the stratosphere, *Science*, 328, 611–613, doi:10.1126/science.1182274, 2010.
- 10 Rauthe-Schöch, A., Baker, A. K., Schuck, T. J., Brenninkmeijer, C. A. M., Zahn, A., Hermann, M., Stratmann, G., Ziereis, H., van Velthoven, P. F. J., and Lelieveld, J.: Trapping, chemistry and export of trace gases in the South Asian summer monsoon observed during CARIBIC flights in 2008, *Atmos. Chem. Phys. Discuss.*, 15, 6967–7018, doi:10.5194/acpd-15-6967-2015, 2015.
- Reddy, R., Gopal, K., Reddy, L., Narasimhulu, K., Kumar, K., Ahammed, Y., and Reddy, C.: Measurements of surface ozone at semi-arid site Anantapur (14.62° N, 77.65° E, 331 m a.s.l.) in India, *J. Atmos. Chem.*, 59, 47–59, doi:10.1007/s10874-008-9094-1, 2008.
- 15 Renuka, K., Gadhavi, H., Jayaraman, A., Lal, S., Naja, M., and Rao, S.: Study of Ozone and NO₂ over Gadanki – a rural site in South India, *J. Atmos. Chem.*, 71, 95–112, doi:10.1007/s10874-014-9284-y, 2014.
- 20 Sahu, L. K. and Lal, S.: Changes in surface ozone levels due to convective downdrafts over the Bay of Bengal, *Geophys. Res. Lett.*, 33, L10807, doi:10.1029/2006GL025994, 2006.
- Saraf, N., and Beig, G.: Long-term trends in tropospheric ozone over the Indian tropical region, *Geophys. Res. Lett.*, 31, doi:10.1029/2003GL018516, 2004.
- Sarangi, T., Naja, M., Ojha, N., Kumar, R., Lal, S., Venkataramani, S., Kumar, A., Sagar, R., and Chandola, H. C.: First simultaneous measurements of ozone, CO, and NO_y at a high-altitude regional representative site in the central Himalayas, *J. Geophys. Res.-Atmos.*, 119, 1592–1611, doi:10.1002/2013JD020631, 2014.
- 25 Scharffe, D., Slemr, F., Brenninkmeijer, C. A. M., and Zahn, A.: Carbon monoxide measurements onboard the CARIBIC passenger aircraft using UV resonance fluorescence, *Atmos. Meas. Tech.*, 5, 1753–1760, doi:10.5194/amt-5-1753-2012, 2012.
- 30 Schell, B., Ackermann, I. J., Hass, H., Binkowski, F. S., and Ebel, A.: Modeling the formation of secondary organic aerosol within a comprehensive air quality model system, *J. Geophys. Res.-Atmos.*, 106, 28275–28293, doi:10.1029/2001JD000384, 2001.

- Schuck, T. J., Brenninkmeijer, C. A. M., Baker, A. K., Slemr, F., von Velthoven, P. F. J., and Zahn, A.: Greenhouse gas relationships in the Indian summer monsoon plume measured by the CARIBIC passenger aircraft, *Atmos. Chem. Phys.*, 10, 3965–3984, doi:10.5194/acp-10-3965-2010, 2010.
- 5 Sheel, V., Lal, S., Richter, A., and Burrows, J. P.: Comparison of satellite observed tropospheric NO₂ over India with model simulations, *Atmos. Environ.*, 44, 3314–3321, doi:10.1016/j.atmosenv.2010.05.043, 2010.
- Shreedharan, C. R.: An Indian electrochemical ozonesonde, *J. Phys. E. Sci. Instrum. Sr.*, 2, 995–997, 1968.
- Smit, H. G. J., and Kley, D.: JOSIE: The 1996 WMO International intercomparison of ozonesondes under quasi flight conditions in the environmental simulation chamber at Jülich, WMO/IGAC-Report, WMO Global Atmosphere Watch report series, No. 130 (Technical Document No. 926). World Meteorological Organization, Geneva, 1998.
- 10 Srinivas, C. V., Hari Prasad, D., Bhaskar Rao, D. V., Baskaran, R., and Venkatraman, B: Simulation of the Indian summer monsoon onset-phase rainfall using a regional model, *Ann. Geophys.*, 33, 1097–1115, doi:10.5194/angeo-33-1097-2015, 2015.
- 15 Srivastava, S., Lal, S., Venkataramani, S., Gupta, S., and Acharya, Y. B.: Vertical distribution of ozone in the lower troposphere over the Bay of Bengal and the Arabian Sea during ICARB-2006: effects of continental outflow, *J. Geophys. Res.-Atmos.*, 116, D13301, doi:10.1029/2010JD015298, 2011.
- 20 Stevenson, D. S., Young, P. J., Naik, V., Lamarque, J.-F., Shindell, D. T., Voulgarakis, A., Skeie, R. B., Dalsoren, S. B., Myhre, G., Berntsen, T. K., Folberth, G. A., Rumbold, S. T., Collins, W. J., MacKenzie, I. A., Doherty, R. M., Zeng, G., van Noije, T. P. C., Strunk, A., Bergmann, D., Cameron-Smith, P., Plummer, D. A., Strode, S. A., Horowitz, L., Lee, Y. H., Szopa, S., Sudo, K., Nagashima, T., Josse, B., Cionni, I., Righi, M., Eyring, V., Conley, A., Bowman, K. W., Wild, O., and Archibald, A.: Tropospheric ozone changes, radiative forcing and attribution to emissions in the Atmospheric Chemistry and Climate Model Intercomparison Project (ACCMIP), *Atmos. Chem. Phys.*, 13, 3063–3085, doi:10.5194/acp-13-3063-2013, 2013.
- 25 Stockwell, W. R., Middleton, P., Chang, J. S., and Tang, X.: The second generation regional acid deposition model chemical mechanism for regional air quality modeling, *J. Geophys. Res.-Atmos.*, 95, 16343–16367, doi:10.1029/JD095iD10p16343, 1990.
- 30 Thompson, G., Field, P. R., Rasmussen, R. M., and Hall, W. D.: Explicit forecasts of winter precipitation using an improved bulk microphysics scheme. part ii: implementation of a new snow parameterization, *Mon. Weather Rev.*, 136, 5095–5115, doi:10.1175/2008MWR2387.1, 2008.

- Tiwari, Y. K., Patra, P. K., Chevallier, F., Francey, R. J., Krummel, P. B., Allison, C. E., Revadekar, J. V., Chakraborty, S., Langenfelds, R. L., Bhattacharya, S. K., Borole, D. V., Ravi Kumar, K., and Paul Steele, L.: Carbon dioxide observations at Cape Rama, India for the period 1993–2002: implications for constraining Indian emissions, *Curr. Sci. India*, 101, 1562–1568, 2011.
- 5 Torres, O., Chen, Z., Jethva, H., Ahn, C., Freitas, S. R., and Bhartia, P. K.: OMI and MODIS observations of the anomalous 2008–2009 Southern Hemisphere biomass burning seasons, *Atmos. Chem. Phys.*, 10, 3505–3513, doi:10.5194/acp-10-3505-2010, 2010.
- Wang, W., Bruyère, C., Duda, M., Dudhia, J., Gill, D., Kavulich, M., Keene, K., Lin, H.-C., Michalakes, J., Rizvi, S., and Zhang, X.: ARW Version 3 Modeling System User's Guide, Chapter 3: WRF Preprocessing System (WPS), NCAR, Boulder, USA, 59–60, 2014.
- 10 WHO: Health Aspects of Air Pollution with Particulate Matter, Ozone and Nitrogen Dioxide, Publisher WHO, Rep. EUR/03/5042688, Bonn, 2003.
- Wiedinmyer, C., Akagi, S. K., Yokelson, R. J., Emmons, L. K., Al-Saadi, J. A., Orlando, J. J., and Soja, A. J.: The Fire INventory from NCAR (FINN): a high resolution global model to estimate the emissions from open burning, *Geosci. Model Dev.*, 4, 625–641, doi:10.5194/gmd-4-625-2011, 2011.
- 15 Worden, H. M., Deeter, M. N., Edwards, D. P., Gille, J. C., Drummond, J. R., and Nédélec, P.: Observations of near-surface carbon monoxide from space using MOPITT multispectral retrievals, *J. Geophys. Res.-Atmos.*, 115, D18314, doi:10.1029/2010JD014242, 2010.
- 20 Yoon, J. and Pozzer, A.: Model-simulated trend of surface carbon monoxide for the 2001–2010 decade, *Atmos. Chem. Phys.*, 14, 10465–10482, doi:10.5194/acp-14-10465-2014, 2014.
- Yoon, J., Pozzer, A., Hoor, P., Chang, D. Y., Beirle, S., Wagner, T., Schloegl, S., Lelieveld, J., and Worden, H. M.: Technical Note: Temporal change in averaging kernels as a source of uncertainty in trend estimates of carbon monoxide retrieved from MOPITT, *Atmos. Chem. Phys.*, 13, 11307–11316, doi:10.5194/acp-13-11307-2013, 2013.
- 25 Zahn, A., Weppner, J., Widmann, H., Schlote-Holubek, K., Burger, B., Kühner, T., and Franke, H.: A fast and precise chemiluminescence ozone detector for eddy flux and airborne application, *Atmos. Meas. Tech.*, 5, 363–375, doi:10.5194/amt-5-363-2012, 2012.
- Zahn, A., Christner, E., van Velthoven, P., F., J., Rauthe-Schöch, A., Brenninkmeijer, C. A. M.: Processes controlling water vapor in the upper troposphere/lowermost stratosphere: An analysis of 8 years of monthly measurements by the IAGOS-CARIBIC observatory, *J. Geophys. Res.*, 119, 11505–11525, doi:10.1002/2014JD021687, 2014.
- 30

Zhang, Q., Streets, D. G., Carmichael, G. R., He, K. B., Huo, H., Kannari, A., Klimont, Z., Park, I. S., Reddy, S., Fu, J. S., Chen, D., Duan, L., Lei, Y., Wang, L. T., Yao, Z. L.: Asian emissions in 2006 for the NASA INTEX-B mission, *Atmos. Chem. Phys.*,9,5131–5153, doi:10.5194/acp-9-5131-2009,2009.

Table 1. The WRF-Chem options used in the present study.

Atmospheric Process	Option used
Cloud microphysics	Thompson microphysics scheme(Thompson et al., 2008)
Longwave radiation	Rapid Radiative Transfer Model (RRTM) (Mlawer et al., 1997)
Shortwave radiation	Goddard shortwave scheme (Chou and Suarez, 1994)
Surface Layer	Monin–Obukhov scheme (Janjic, 1996)
Land-surface option	Noah Land Surface Model (Chen and Dudhia, 2001)
Urban surface physics	Urban Canopy Model
Planetary boundary layer	Mellor–Yamada–Janjic scheme (Janjic, 2002)
Cumulus parametrization	New Grell scheme (G3)
Gas Phase chemistry	RADM2
Aerosol module	MADE SORGAM

Table 2. Description of WRF-Chem simulations performed for this study.

Simulation Name	Description
(1) Std	WRF-Chem simulations driven by MOZART4/GEOS5 boundary conditions. No factor on boundary conditions or emissions. This simulation is used as the standard WRF-Chem run for this study.
(2) Std_INTEX	Similar to Std run, except anthropogenic emissions from a different inventory (INTEX-B)
(3) 1.5×_EM	The anthropogenic emissions of CO over the entire South Asian domain have been increased by 50 %, everything else fixed same as for Std.
(4) 1.25×_BDY	CO in MOZART-GEOS5 boundary conditions increased by 25 % over a region at the western boundary of the domain, as shown in Fig. 13, everything else fixed same as for Std.

Table A1. Abbreviations/Acronym.

ARCTAS:	Arctic Research of the Composition of the Troposphere from Aircraft and Satellites
CARIBIC:	Civil Aircraft for the Regular Investigation of the Atmosphere Based on an Instrument Container
CFL:	Courant-Friedrichs-Levy
EDGAR:	Emission Database for Global Atmospheric Research
EMEP:	European Monitoring and Evaluation Programme
EPA:	Environmental Protection Agency
EOS:	Earth Observing System
FNL GFS:	Final analysis Global Forecast System
GEOS5:	Goddard Earth Observing System Model, Version 5
GOCART:	Goddard Chemistry Aerosol Radiation and Transport
HYSPLIT:	Hybrid Single Particle Lagrangian Integrated Trajectory
HTAP:	Hemispheric Transport of Air Pollution
IGP:	Indo-Gangetic Plain
INTEX-B:	Intercontinental Chemical Transport Experiment Phase B
MADE:	Modal Aerosol Dynamics Model for Europe
MATCH-MPIC:	Model of Atmospheric Transport and Chemistry – Max Planck Institute for Chemistry version
MERRA:	Modern Era-Retrospective Analysis for Research and Applications
MICS:	Model Intercomparison Study
MOPITT:	Measurements of Pollution in the Troposphere
MOZART:	Model for OZone and Related chemical Tracers
NCEP:	National Centers for Environmental Prediction
NCAR:	National Center for Atmospheric Research
RADM2:	Regional Acid deposition Model Second Generation
REAS:	Regional Emission inventory in ASia
RMSD:	Root Mean Square Deviation
SORGAM:	Secondary Organic Aerosol Model
WRF-Chem:	Weather Research and Forecasting with Chemistry

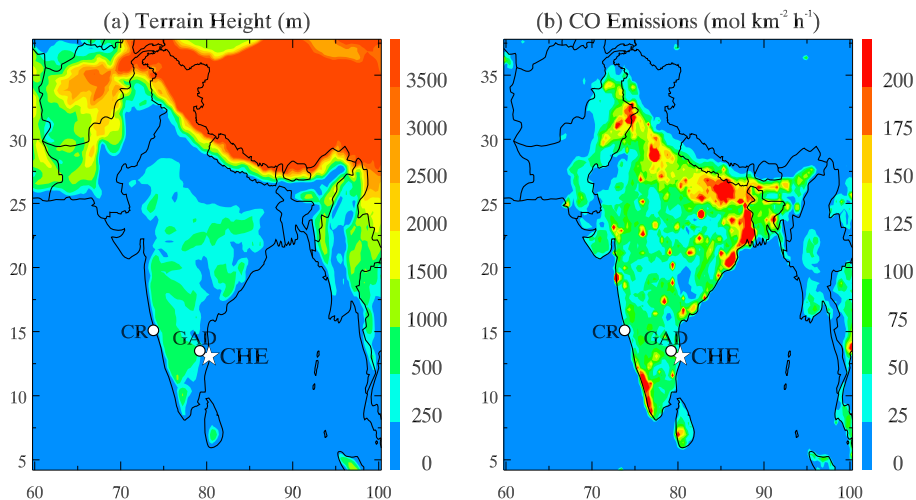


Figure 1. (a) The simulation domain of WRF-Chem covering the South Asian region at a spatial resolution of $30\text{ km} \times 30\text{ km}$, including topography map. (b) Anthropogenic emissions of CO over the South Asian region for June 2008 from the HTAP v2.2 emission inventory. The location of Chennai (CHE) is shown over which the profiles have been measured as a part of the CARIBIC program. Cape Rama (CR) and Gadanki (GAD) are two additional sites for which ground-based measurements have been used. The three ozonesonde stations Delhi (DEL), Pune (PUN) and Thiruvananthapuram (TVM) are also shown.

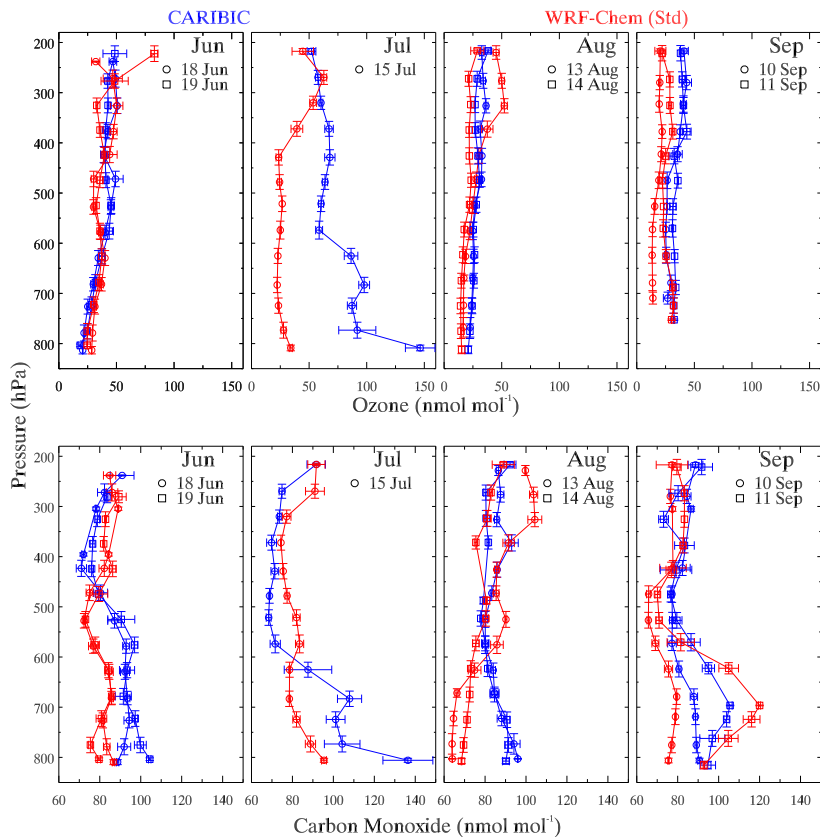


Figure 2. Comparison of Ozone and Carbon Monoxide profiles from WRF-Chem simulations (Std, red lines) with the CARIBIC observations (blue lines) during June, July, August and September 2008. Model output has been spatially and temporally interpolated along the CARIBIC flight tracks. Only data collected during the aircraft descent is shown here (see Sect. 4.1.1 for details).

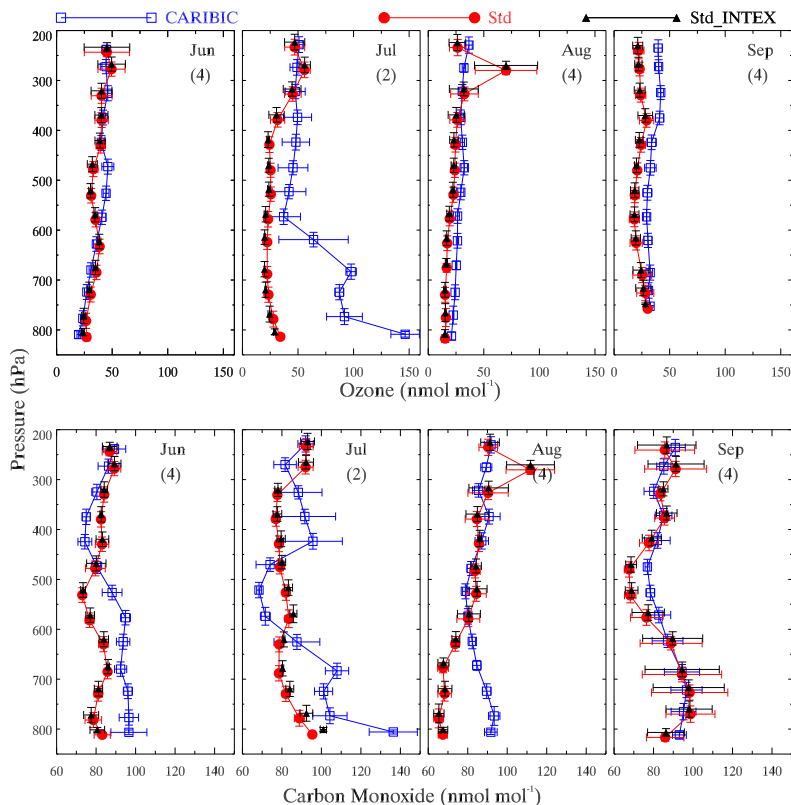


Figure 3. Comparison of monthly average ozone and carbon monoxide profiles from standard WRF-Chem simulations (Std) with the CARIBIC observations during June, July, August and September 2008. Numbers in brackets denote the number of observational profiles in the respective month. Model output has been spatially and temporally interpolated along the CARIBIC flight tracks. Comparison with another simulation Std_INTEX is indicated in black.

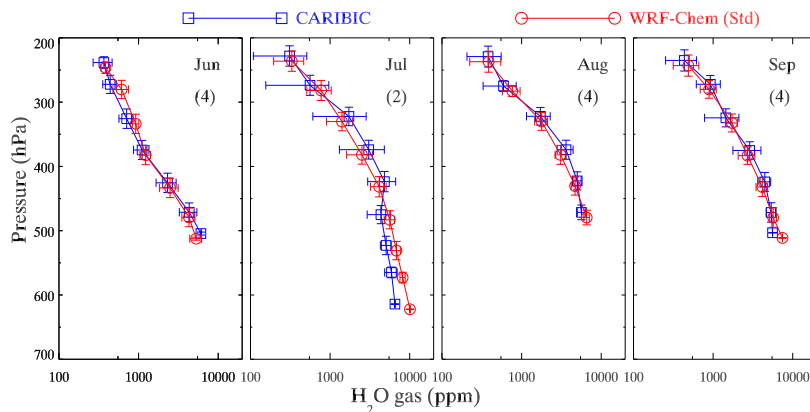


Figure 4. Comparison of monthly average H_2O gas (ppm) from standard WRF-Chem simulations (Std) with the CARIBIC observations during June, July, August and September 2008. Numbers in brackets denote the number of observational profiles in the respective month. Model output has been spatially and temporally interpolated along the CARIBIC flight tracks. Note the logarithmic scale on the X axis.

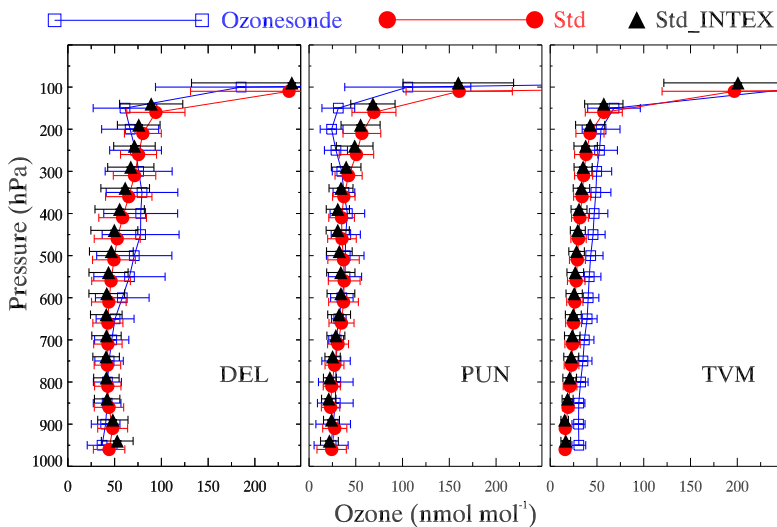


Figure 5. Comparison of average ozone mixing ratios during the summer monsoon (June-September) from Std and Std_INTEX WRF-Chem simulations (Std) with the ozonesonde observational climatology during 2006-2009 period over Delhi (DEL), Pune (PUN) and Thiruvananthapuram (TVM).

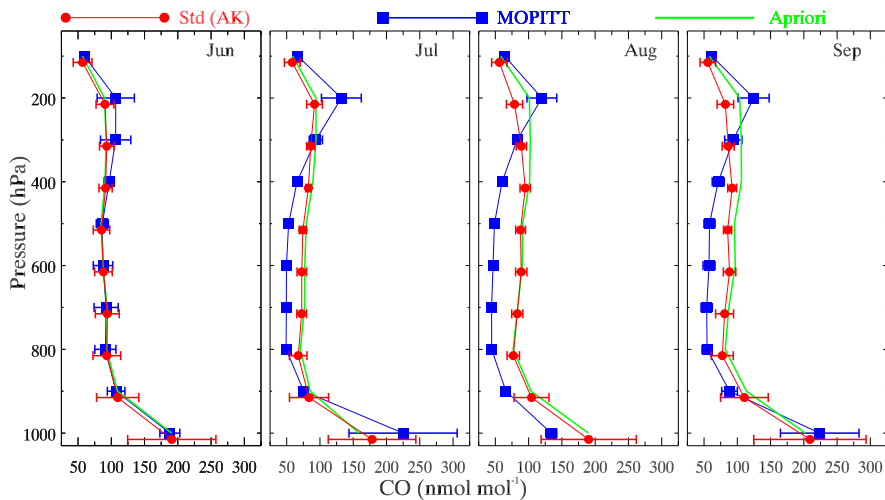


Figure 6. Comparison of monthly average CO from WRF-Chem simulations (Std) with the MOPITT retrievals over Chennai during the four months of the summer monsoon period of the year 2008. The MOPITT averaging kernel and the a priori profile have been applied to the WRF-Chem output, denoted by Std (AK). MOPITT a priori profile is also shown for comparison.

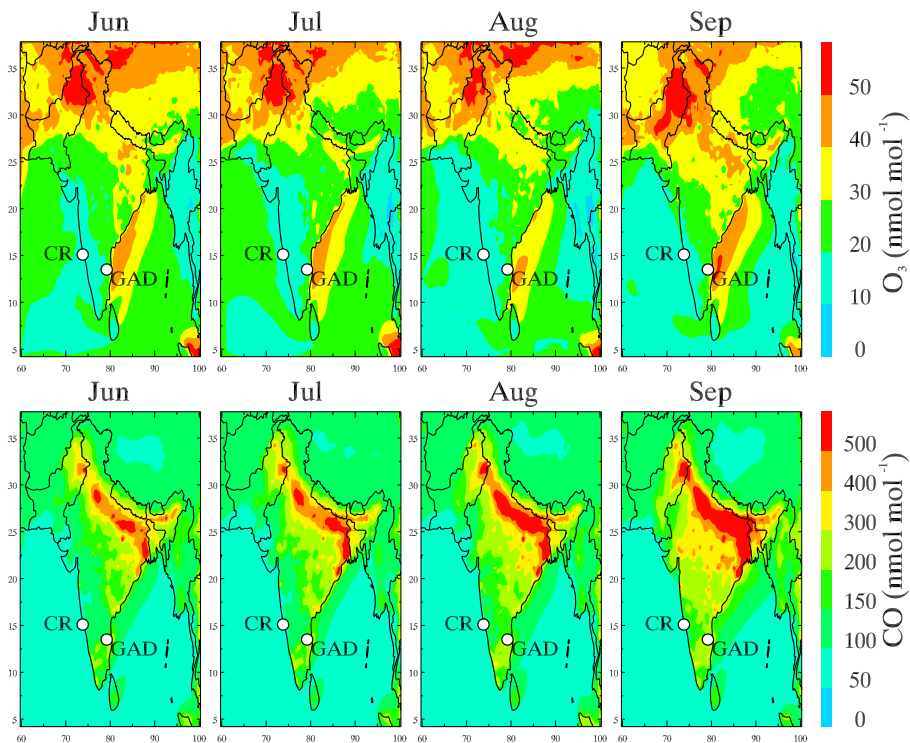


Figure 7. Spatial distribution of monthly average surface ozone and CO (nmol mol^{-1}) from WRF-Chem simulations (Std) during June, July, August and September 2008. The locations of two surface sites, Cape Rama (CR) and Gadanki (GAD), are also shown.

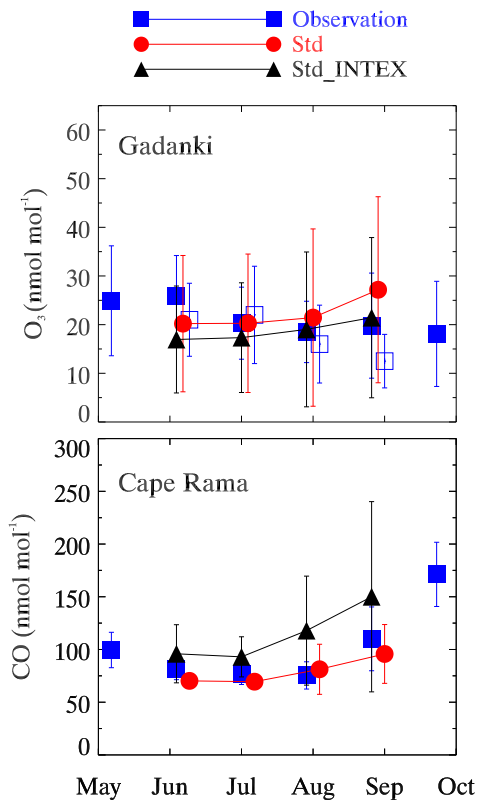


Figure 8. Comparison of WRF-Chem simulated surface ozone and CO with the ground-based measurements at Gadanki (79.2° E, 13.5° N) (Naja and Lal, 2002) and Cape Rama (73.8° E, 15.1° N). Open blue symbols for Gadanki show observations from another study (Renuka et al., 2014). Comparison with Std_INTEX simulation is indicated in black.

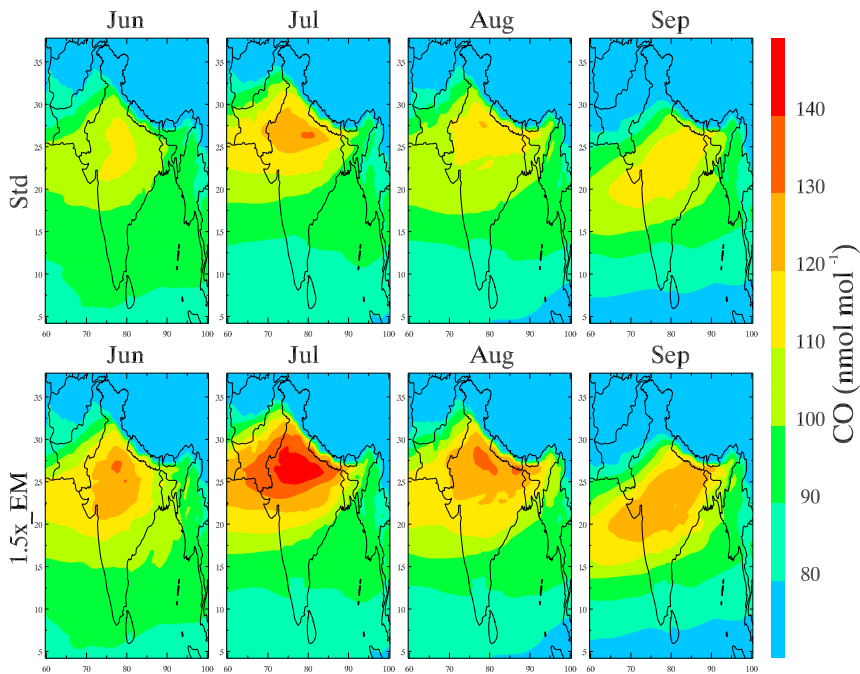


Figure 9. Comparison of monthly average horizontal distribution of CO in the upper troposphere (116 hPa to 211 hPa) over India from the Std simulation (top panel) and $1.5\times_EM$ simulation (bottom panel) during June, July, August and September 2008.

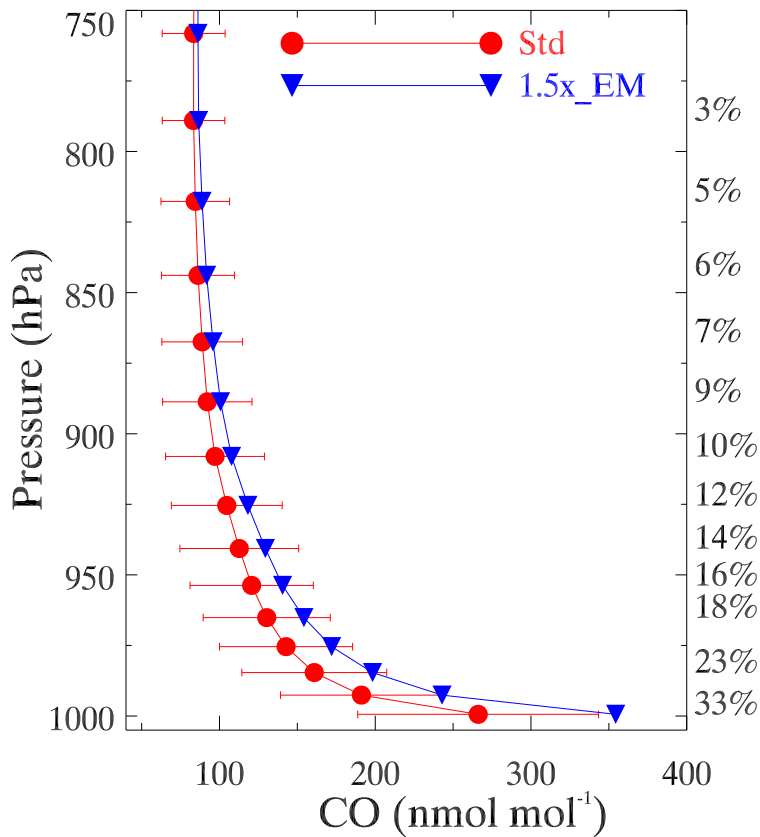


Figure 10. Monthly average vertical profile of CO over Chennai during June from Std and 1.5 \times _EM simulations. The resulting enhancement in CO is also indicated in percentages along the right axis.

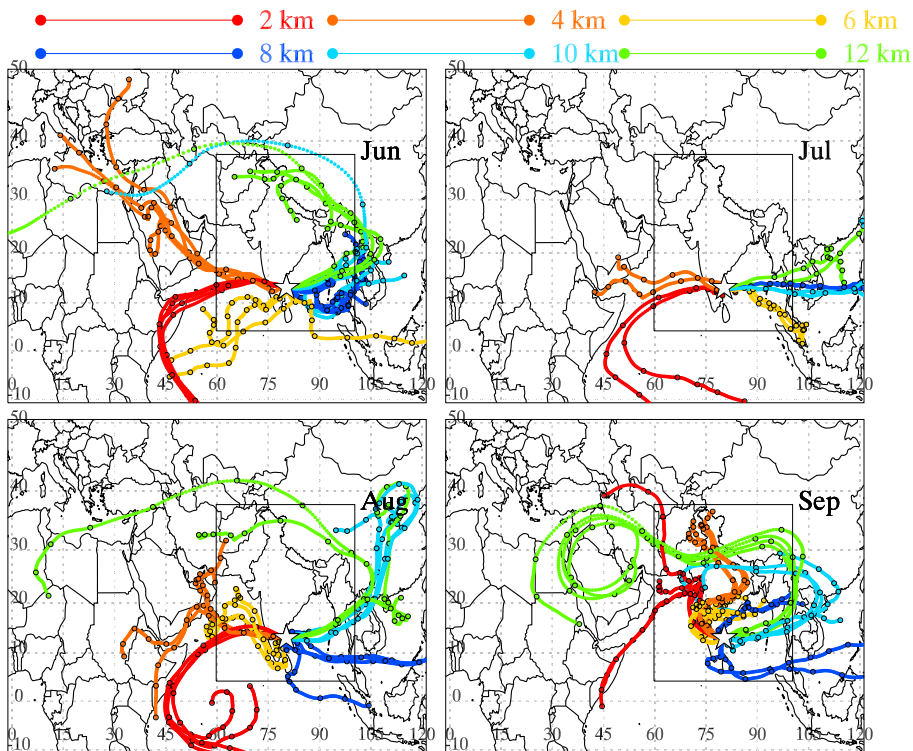


Figure 11. HYSPLIT simulated 10 days backward air trajectories at 2, 4, 6, 8, 10 and 12 km a.s.l. over Chennai for the CARIBIC measurement days. Different colors of trajectories correspond to different starting altitude over Chennai for the trajectory simulations.

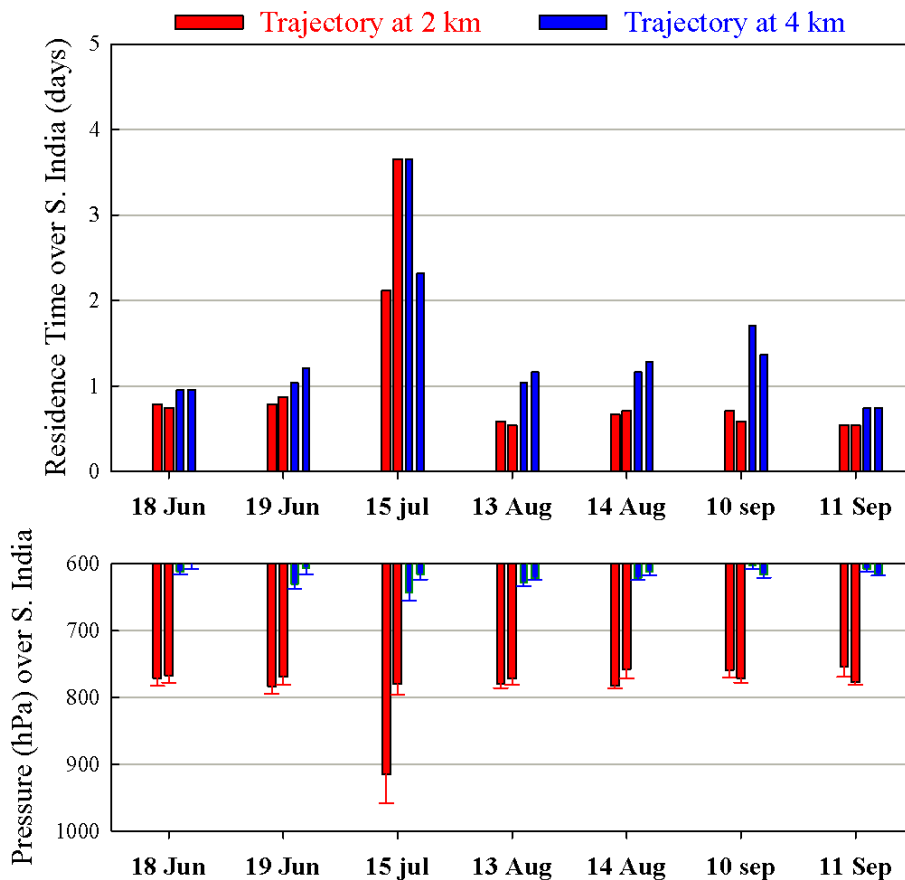


Figure 12. Residence time of air masses over the southern Indian region on all CARIBIC measurement days calculated from the back-trajectories at 2 and 4 km above Chennai. The mean pressure along the trajectory over southern India is also shown.

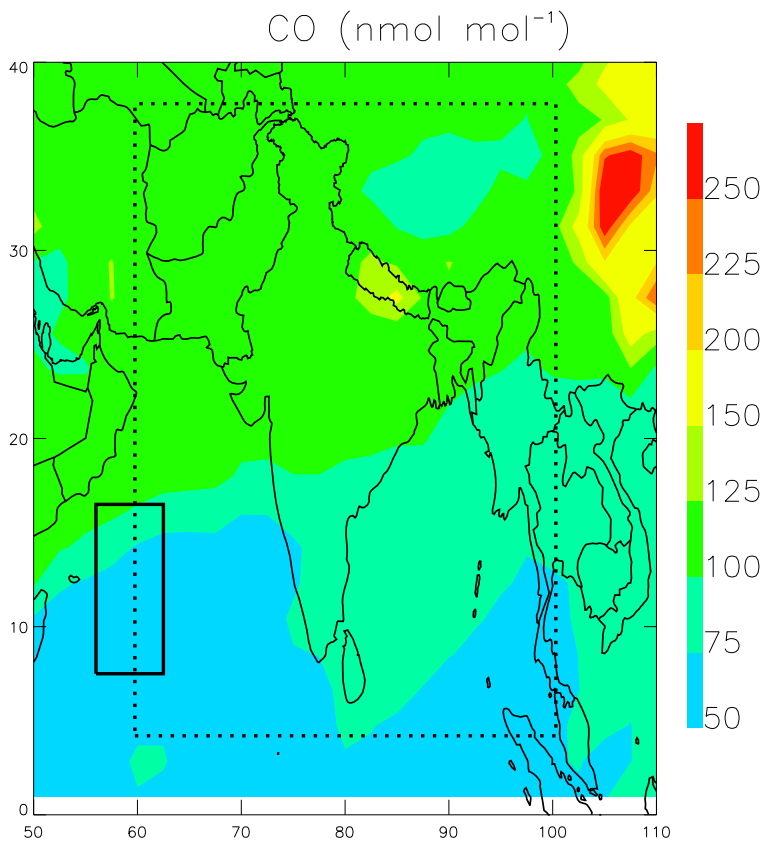


Figure 13. Spatial distribution of CO at 810 hPa from MOZART GEOS5 boundary condition data on a typical day (18 June 2008 at 18:00 GMT). The WRF-Chem simulation domain is shown as the dotted box. The CO mixing ratios over part of the western boundary, shown by the thick solid box, have been increased by 25 % in the simulation $1.25 \times \text{BDY}$.

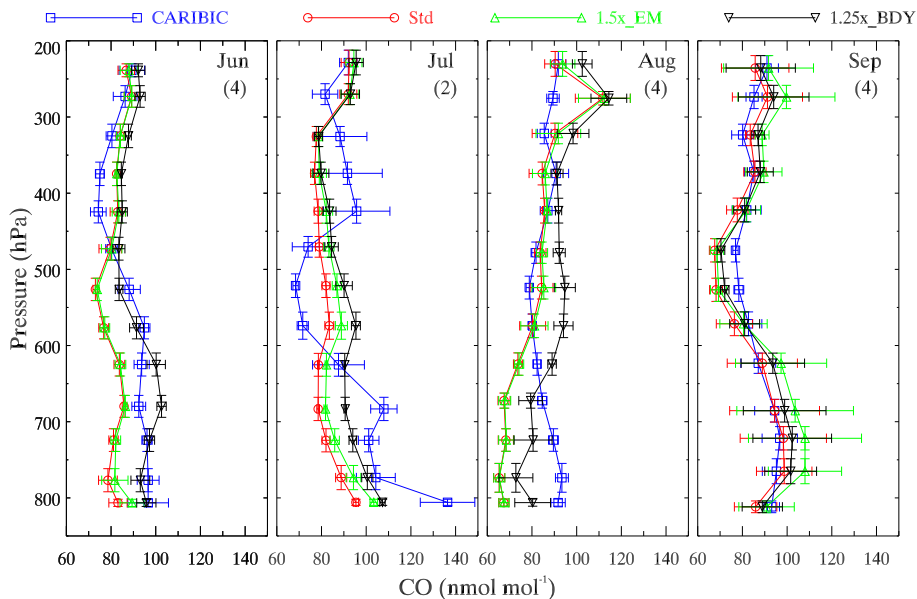


Figure 14. Sensitivity analysis of WRF-Chem simulated CO profiles to the chemical boundary conditions. Standard CO profiles are compared with the simulation driven by 25 % higher CO at the western boundary of the domain as shown in Fig. 13. Results from 50 % higher CO emissions over the whole domain ($1.5\times_EM$) are also shown for comparison. Numbers in brackets denote the number of observational profiles in the respective month.